

Contents lists available at ScienceDirect

Journal of Rock Mechanics and Geotechnical Engineering

journal homepage: www.jrmge.cn



Full Length Article

Solving fluid flow in discontinuous heterogeneous porous media and multi-layer strata with interpretable physics-encoded finite element network



Xi Wang a, b, Wei Wu a, c, d, *, He-Hua Zhu a, c, d

- ^a College of Civil Engineering, Tongji University, Shanghai, 200092, China
- b Department of Civil and Environmental Engineering, The Hong Kong Polytechnic University, Hung Hom, Kowloon, 999077, Hong Kong, China
- ^c State Key Laboratory of Disaster Reduction in Civil Engineering, Tongji University, Shanghai, 200092, China
- d Key Laboratory of Geotechnical and Underground Engineering of Ministry of Education, Tongji University, Shanghai, 200092, China

ARTICLE INFO

Article history: Received 30 May 2024 Received in revised form 4 October 2024 Accepted 24 October 2024 Available online 31 December 2024

Keywords:
Finite element method (FEM)
Physics-informed neural network (PINN)
Carbon neutrality
Sheet pile
Sharp/steep gradients
Porous flow

ABSTRACT

Physics-informed neural networks (PINNs) have prevailed as differentiable simulators to investigate flow in porous media. Despite recent progress PINNs have achieved, practical geotechnical scenarios cannot be readily simulated because conventional PINNs fail in discontinuous heterogeneous porous media or multi-layer strata when labeled data are missing. This work aims to develop a universal network structure to encode the mass continuity equation and Darcy's law without labeled data. The finite element approximation, which can decompose a complex heterogeneous domain into simpler ones, is adopted to build the differentiable network. Without conventional DNNs, physics-encoded finite element network (PEFEN) can avoid spectral bias and learn high-frequency functions with sharp/steep gradients. PEFEN rigorously encodes Dirichlet and Neumann boundary conditions without training. Benefiting from its discretized formulation, the discontinuous heterogeneous hydraulic conductivity is readily embedded into the network. Three typical cases are reproduced to corroborate PEFEN's superior performance over conventional PINNs and the PINN with mixed formulation. PEFEN is sparse and demonstrated to be capable of dealing with heterogeneity with much fewer training iterations (less than 1/30) than the improved PINN with mixed formulation. Thus, PEFEN saves energy and contributes to low-carbon AI for science. The last two cases focus on common geotechnical settings of impermeable sheet pile in singlelayer and multi-layer strata. PEFEN solves these cases with high accuracy, circumventing costly labeled data, extra computational burden, and additional treatment. Thus, this study warrants the further development and application of PEFEN as a novel differentiable network in porous flow of practical geotechnical engineering.

© 2025 Institute of Rock and Soil Mechanics, Chinese Academy of Sciences. Published by Elsevier B.V. This is an open access article under the CC BY-NC-ND license (http://creativecommons.org/licenses/by-nc-nd/4.0/).

1. Introduction

Deep neural networks (DNNs) have achieved remarkable progress in various domains including geoengineering (Chen et al., 2024), large language models, and policy learning. Artificial intelligence is acting like the "new electricity" to offer new power for traditional domains in science and engineering. Conventional numerical methods such as the finite element method (FEM)

E-mail address: weiwu@tongji.edu.cn (W. Wu).

(Zienkiewicz et al., 2005), finite difference method (FDM) (Forsythe and Wasow, 1960), material point method (Liang and Zhao, 2019; Liang et al., 2024; Yu et al., 2024a), peridynamics (Silling and Lehoucq, 2010; Ren et al., 2017; Yang et al., 2024a, 2024b), and discontinuous deformation analysis (Shi, 1992; Wang et al., 2019, 2022) are important tools to analyze and predict complex natural and engineering phenomena. Li et al. (2020a, 2021) proposed a grain-based method (in hybrid finite discrete element method) modeling rock microstructures, revealing how they affect crack thresholds and nonlinear deformation, offering a new potential solution and insights into fracturing and cross-scale mechanical behaviors in rocks. Xu et al. (2019, 2020a) discovered mechanical behaviors of isotropic rocks with the discrete element method and

^{*} Corresponding author. College of Civil Engineering, Tongji University, Shanghai, 200092, China.

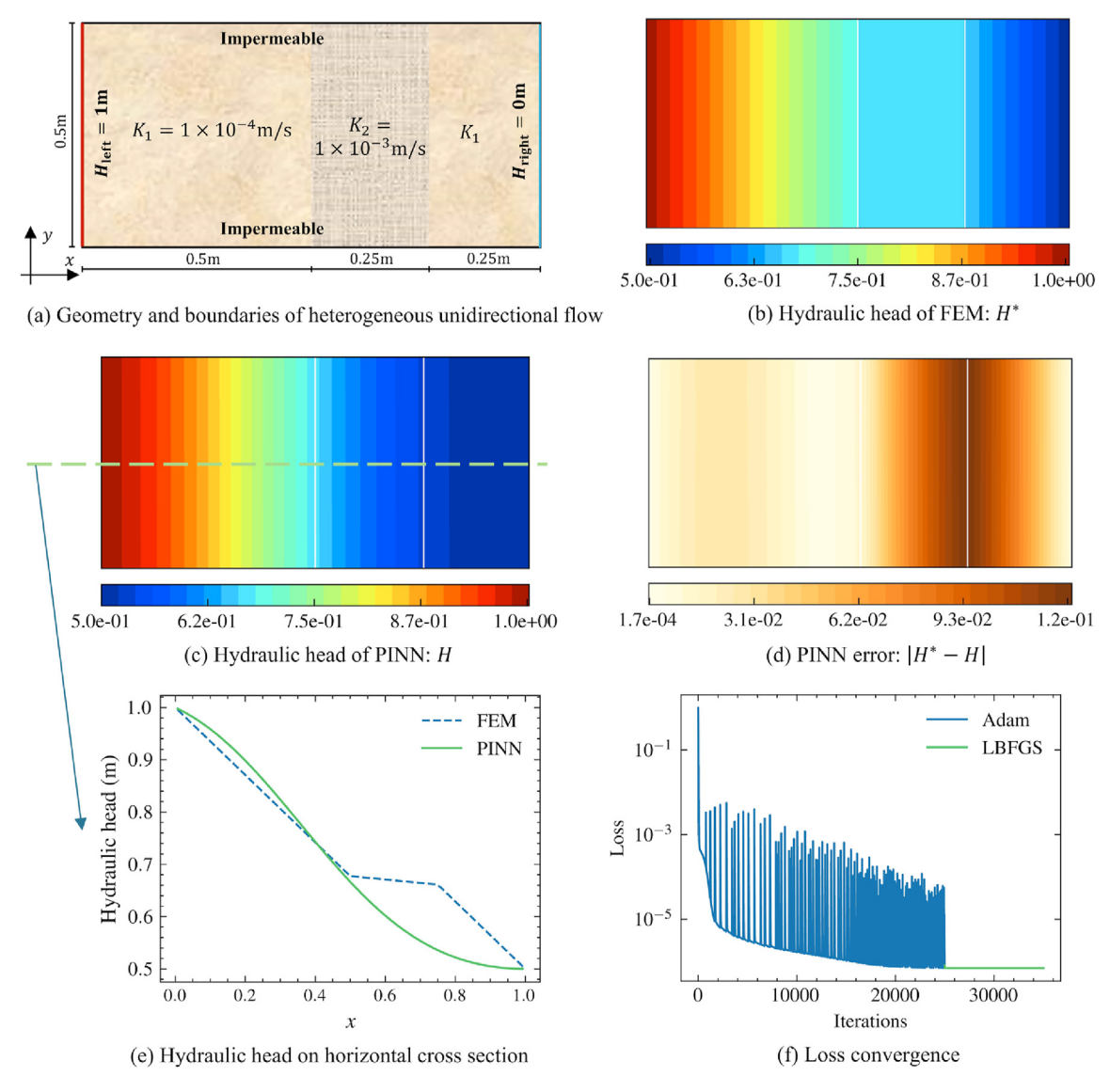


Fig. 1. Solving flow in discontinuous heterogeneous porous media using PINN.

laboratory tests. Li et al. (2020a, b) and Wei et al. (2021) applied FDM and FEM to analyze rock masses considering structural characteristics. Recent trends show physics-based simulations capturing solid skeleton behavior, offering a promising alternative for multiphysics analysis without constitutive assumptions (Liang et al., 2023; Yu et al., 2024b). DNNs, on the other hand, provide a new paradigm for computational methods. DNNs have been widely applied for constitutive modeling (Qu et al., 2023; Wang et al., 2024), solid mechanics (Abueidda et al., 2021; Haghighat et al., 2021b; Bai et al., 2023), and fluid mechanics (Mao et al., 2020; Rao et al., 2023).

The physics we focus on is the fluid flow in porous media, which plays a critical role in various engineering applications such as urban flood mitigation through porous asphalt pavement (Yang et al., 2022), dam seepage, enhanced geothermal systems, geological carbon storage, radioactive waste disposal (Zhuang et al., 2024), and unconventional oil/gas reservoirs. The data-driven DNNs have been applied to model fluid flow and transport in porous media. Laloy et al. (2018) used a generative adversarial network to train a very low dimensional parameterization for efficient sampling and probabilistic inversion of complex geologic media. Kreyenberg et al. (2019) trained a convolutional neural network (CNN) on numerical

simulation to estimate velocity fields. Wu et al. (2019) trained a CNN to map images to diffusivity of porous media computed with lattice Boltzmann simulations. Sun et al. (2022) compared three data-driven DNNs to predict groundwater levels. Rajabi et al. (2022) investigated an encoder-decoder CNN to learn image-to-image correlations for forward and inverse analyses of convection and temperature distribution. Virupaksha et al. (2024) trained encoder-decoder CNN and long short-term memory (LSTM) networks for transient convection. Some other works also incorporate data-driven DNNs as efficient surrogates for inverse analysis (Zhu and Zabaras, 2018; Mo et al., 2019a; Tang et al., 2021) or uncertainty quantification (Mo et al., 2019b).

As surrogate models, data-driven DNNs can efficiently alleviate the curse of dimensionality (Mo et al., 2019a). However, an accurate and robust data-driven DNN surrogate entails a large amount of labeled data for training and testing. Acquiring enough labeled data may be costly and time-consuming if relying on intensive computation with classical numerical methods. From engineering field monitoring or scientific experiments, the labeled data may be even unaffordable and inaccessible. Extrapolation and prediction of data with unseen distributions are also nontrivial challenges for data-driven DNNs because generalized physics is not honored.

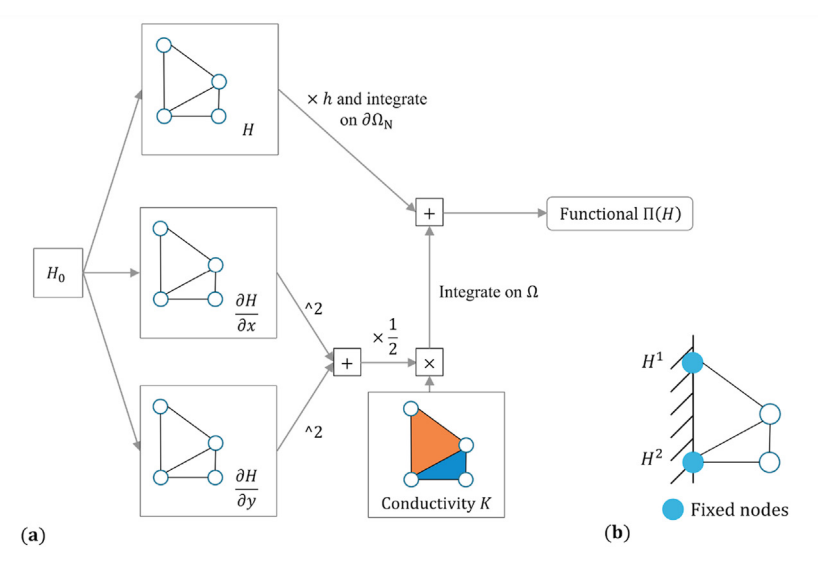


Fig. 2. Overview of the physics-encoded finite element network (PEFEN) for porous flow.

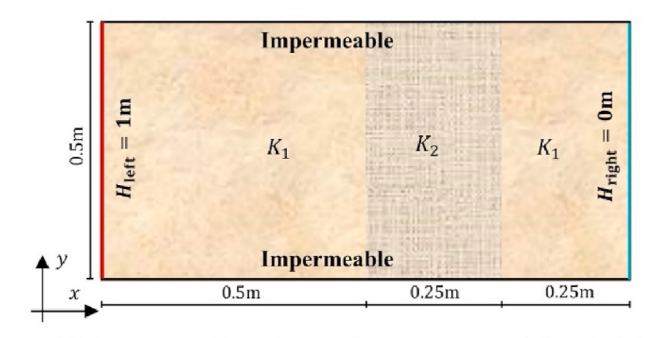
Recently, physics-informed neural networks (PINNs) have been developed to incorporate the residuals of partial differential equations (PDEs) into the loss function of DNNs (Raissi et al., 2019). PINNs conform to physics by minimizing PDE residuals. Data and physics are seamlessly combined by adding PDE residuals and data losses together, thereby facilitating data assimilation and inverse analysis (Karniadakis et al., 2021). For example, the temporal graph neural network-based simulator enhances interpretability by integrating physical information flow constraints into its architecture (Zhao et al., 2024), unlike conventional methods focusing only on loss functions. Physics-informed machine learning methods have also been leveraged in structural health monitoring, inverse analysis, and concrete optimization (Sun et al., 2023, 2024; Li et al., 2024; Luo et al., 2024a, 2024b). Yang et al. (2024c) developed adaptive task decomposition physics-informed neural networks to solve complex time-dependent tasks.

PINNs are attracting increasing interest in modeling flow in porous media. Wang et al. (2020) incorporated PDE residuals, data losses, and engineering controls/expert knowledge (penalty for out-of-range values) to learn the transient saturated flow. With partial measurements and PDE losses. Tartakovsky et al. (2020) trained DNNs for saturated and unsaturated flows. Bandai and Ghezzehei (2021) constrained DNNs to be monotonic to learn constitutive relations in unsaturated flow from noisy data and PDE residuals. Almajid and Abu-Al-Saud (2022) found that PINN outperformed the data-driven DNN when only partial data were available in multiphase flow. Yeung et al. (2022) extended the physics-informed conditional machine learning method for largescale data assimilation of Darcy flow. Guo et al. (2023) proposed a hydraulic tomography-physics-informed neural network to invert Gaussian transmissivity fields of Darcy flow with pumping. Based on PINN, Elkhadrawi et al. (2024) solved unsaturated flow with sparse labeled data to estimate homogeneous hydraulic conductivity. These examples validated PINNs as effective tools to reduce data requirement and perform inverse analysis.

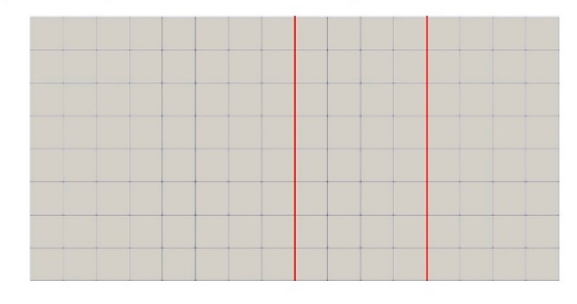
However, the performance of PINN is not perfect. There are multiple terms in the loss function of PINN, including discrepancies from labeled data, PDE residuals, and constraints of boundary conditions. Varying the coefficient might lead to a complex loss landscape, gradient pathology, and optimization issues (Krishnapriyan et al., 2021; Wang et al., 2021). Spectral bias also prevents PINNs with conventional DNNs from learning high-

frequency functions (Rahaman et al., 2019). Moreover, most existing PINN studies entail enough labeled data, which can be inaccessible for science and engineering. In homogeneous porous flow, it was reported that "training PINNs is very slow and control over its accuracy is challenging" (Haghighat et al., 2022).

This study focuses on PINNs without labeled data. For example, Daolun et al. (2021) added a gradient model as special neurons in the hidden layer of PINN to solve Darcy seepage with source/sink terms. Zhang et al. (2022) adopted locally refined sampling strategy for spatial sampling and snowball-style two-stage training strategy to divide temporal domain for Darcy flow. Hanna et al. (2022) developed a residual-based adaptive PINN to better capture moving flow fronts with two phases in the absence of labeled data. Lan



(a) Geometry and boundaries of heterogeneous unidirectional flow



(b) PEFEN mesh

Fig. 3. Configuration of the unidirectional flow in a heterogeneous domain.

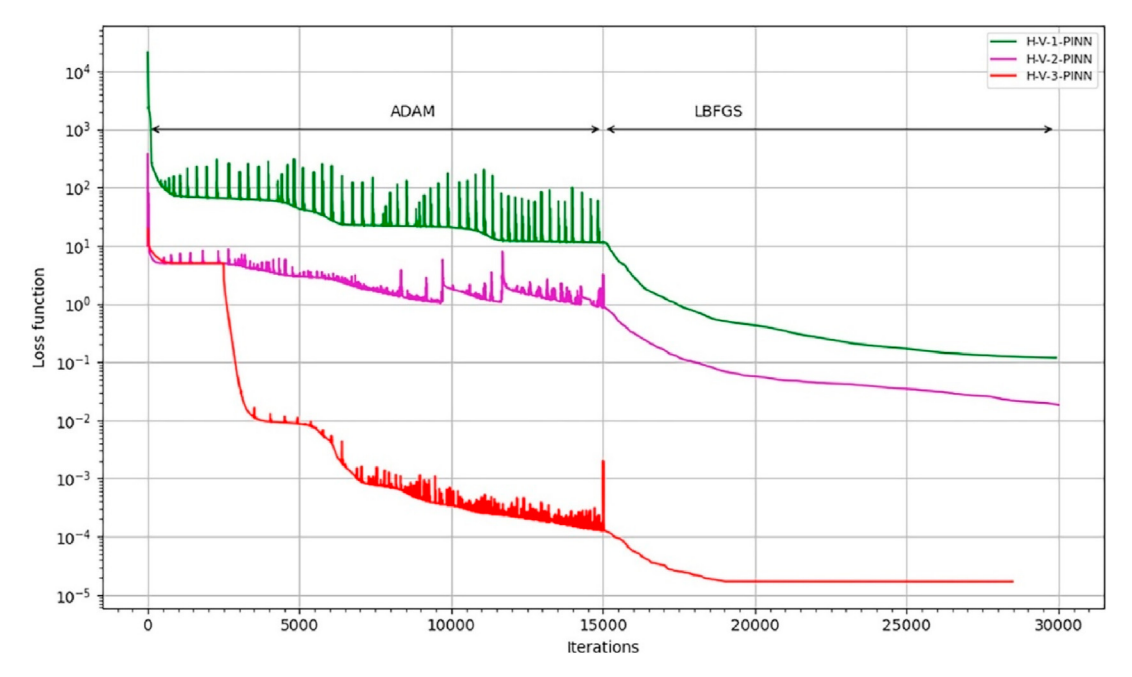


Fig. 4. Loss convergence of mixed-form PINN, reprinted from Fig. 6 in Lehmann et al. (2023): Convergence of H-V-1-PINN, H-V-2-PINN, and H-V-3-PINN in the case of heterogeneous domain: Variation of the loss function with respect to the number of iterations with Adam optimizer (15,000 iterations) followed by LBFGS.

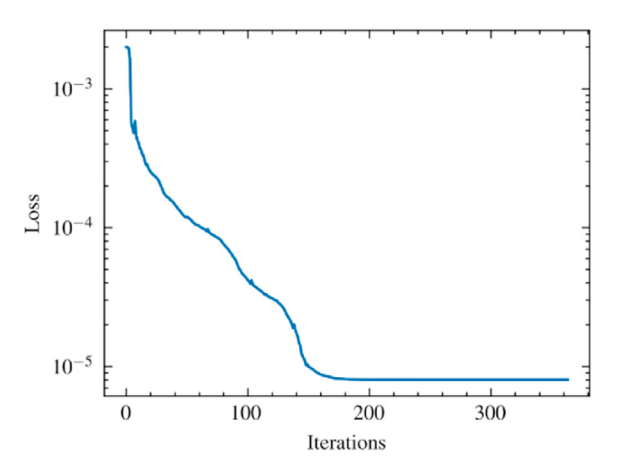


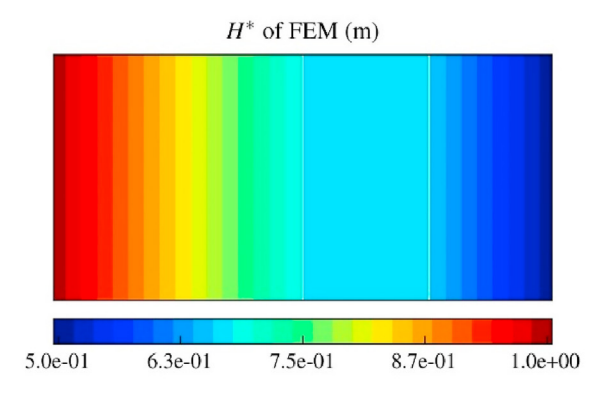
Fig. 5. PEFEN loss convergence in the case of unidirectional flow in a heterogeneous domain.

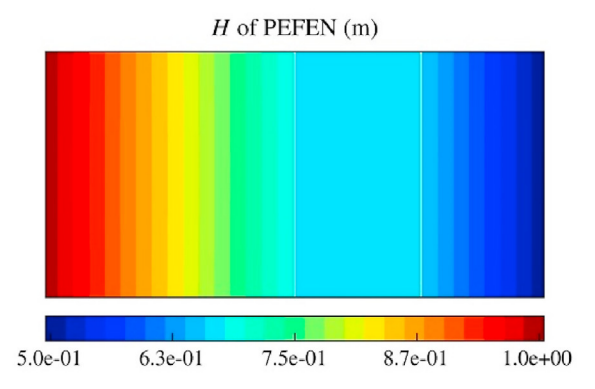
et al. (2023) used an augmented Lagrangian method to constrain initial and boundary conditions without other labeled data for unsaturated flow.

Despite the improvement of PINNs as forward solvers for porous flow without labeled data, its application toward practical geotechnical settings is prohibitive when considering (discontinuous) high heterogeneity. A probable reason is that discontinuous hydraulic conductivity can result in the failure of automatic differentiation. Thus, He et al. (2020) added an extra network to learn heterogeneous hydraulic conductivity, in which the discontinuous interface is smoothly approximated. An alternative is to use a continuous analytical expression to control the heterogeneity or use mild continuous heterogeneity (Tartakovsky et al., 2020; Wang et al., 2020; Yeung et al., 2022; Secci et al., 2024).

Some endeavors are committed to solving discontinuous and high heterogeneity without costly labeled data in porous flow. A straightforward and effective way is to decompose the heterogeneous domain into homogeneous subdomains (Bandai and Ghezzehei, 2022). Diao et al. (2023) developed domain decomposition technology to solve mult-material problems. In this method, subnetworks should be defined on subdomains, and additional treatments are necessary for interfaces. Zhang et al. (2022, 2023) applied finite volume discretization to compute the derivatives from CNN for Darcy flow, and a relatively low resolution was adopted for efficiency. With extra variables, Lehmann et al. (2023) developed a mixed-form PINN to simulate Darcy flow without any additional treatments or assumptions.

The challenges associated with the performance of PINNs in heterogeneous cases can also be attributed to the properties of DNNs. The F-principle/spectral bias stated that "DNNs tend to fit training data by a low-frequency function" and "F-principle results from the smoothness/regularity of the commonly used activation functions" (Xu et al., 2020b). Thus, this study employs a novel physics-encoded finite element network (PEFEN), instead of conventional DNNs, to approximate the field variable to handle discontinuous and highly heterogeneous porous flow. PEFEN is recently proposed to solve nonlinear elasticity (Wang and Yin, 2024). PEFEN decomposes highly heterogeneous domains into simpler and less heterogeneous ones. It can also fit complex functions without activation functions. Thus, PEFEN can naturally encode heterogeneous hydraulic conductivity without additional special treatment, extra variables, or labeled data. The Dirichlet boundary conditions can be encoded into the discretized mesh in PEFEN, and Neumann boundary conditions are considered by its work. Importantly, no labeled data are required, and the loss function consists solely of the functional. Thus, the problem of imbalanced losses and gradient pathology can be alleviated in PEFEN. Another challenge of AI is the computational cost and resources. PEFEN can be considered as a sparse network that entails much fewer iterations to converge. As suggested by Guan (2024), development of PEFEN is beneficial for carbon neutrality. Compared with existing works leveraging FEM with PINN (Gao et al., 2022; Wang et al., 2024), PEFEN circumvents the dependence on conventional DNNs and features sparse network for efficient training and heterogeneous problems.





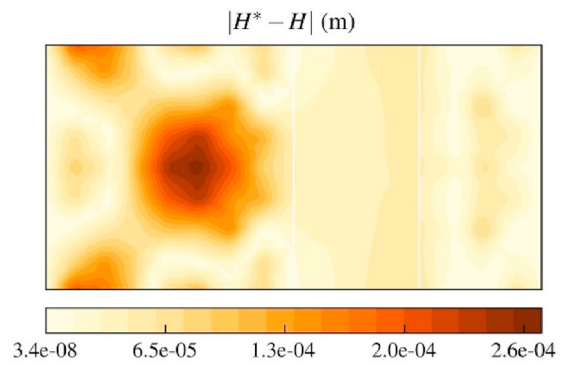


Fig. 6. Comparison of hydraulic head from FEM and PEFEN in the case of unidirectional flow in a heterogeneous domain.

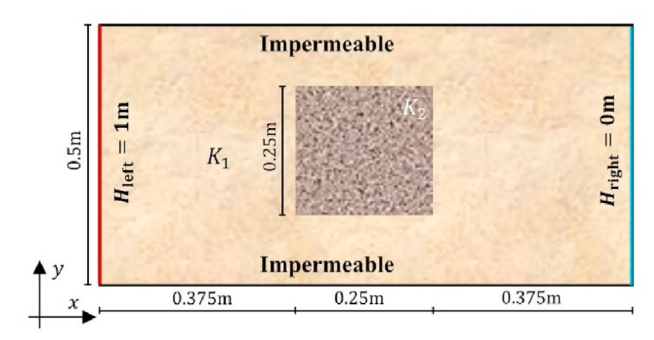
The paper is organized as follows. First, the fundamentals of PINNs and the challenges associated with heterogeneous porous domains are briefly reviewed. Next, the methodology of PEFEN is introduced. Three numerical experiments are conducted to validate the accuracy of PEFEN when dealing with heterogeneity. The significantly faster convergence of PEFEN compared to the mixed-form PINN is also demonstrated. The last two cases prove PEFEN capable of solving more practical cases in single-layer and multi-layer strata with an impermeable sheet pile.

2. PINN and challenges of simulating flow in heterogeneous domains

Darcy's law is the constitutive relation between hydraulic head and Darcy velocity:

$$v = K(x, y)\nabla H \tag{1}$$

where the hydraulic conductivity K(x,y) (m/s) is a function of



(a) Geometry and boundaries of heterogeneous bi-directional flow

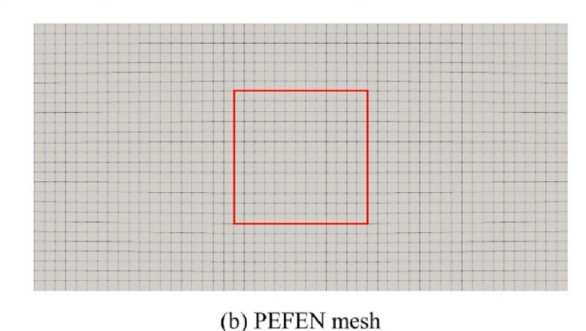


Fig. 7. Configuration of bi-directional flow in a heterogeneous domain.

spatial coordinates, the gradient of hydraulic head H (m) constitutes the driving force of fluid flow, and v (m/s) is the Darcy velocity. According to the continuity equation, the divergence of the Darcy velocity field is zero (assuming the sink/source is zero):

$$\nabla \cdot v = 0 \tag{2}$$

Substituting Eq. (1) into Eq. (2), the governing equation leads to

$$\nabla \cdot (K(x, y)\nabla H) = 0 \tag{3}$$

Dirichlet boundary conditions on $\partial \Omega_D$ and Neumann boundary conditions on $\partial \Omega_N$ are defined as follows:

$$H(x,y) = g \text{ (on } \partial \Omega_{D}) \tag{4}$$

$$\nu(\mathbf{x}, \mathbf{y}) \cdot \mathbf{n} = h \text{ (on } \partial \Omega_{\mathbf{N}}) \tag{5}$$

PINNs predict hydraulic head $\widehat{H}(x,y)$ approximately with neural networks as follows:

$$\widehat{H}(x,y) = (A_{n_l} \circ \sigma_{n_l-1} \circ A_{n_l-1} \circ \cdots \circ \sigma_1 \circ A_1)(x,y)$$
(6)

where 'o' is the composition operator, A_i $(1 \le i \le n_l)$ is the ith linear layer, and σ_i $(1 \le i \le n_l - 1)$ is the neuron-wise activation function. For a commonly used fully connected neural network, the linear layer is as follows:

$$A_i(x) = W_i x + b_i \tag{7}$$

A commonly used activation function with continuous derivative is

$$\sigma_i(x) = \tanh(x) = \frac{e^x - e^{-x}}{e^x + e^{-x}}$$
 (8)

Substituting Eq. (6) into Eq. (3), the resulting residuals at meshless sampling points are incorporated into the loss function of PINNs. Residuals from boundary conditions in Eqs. (4) and (5)

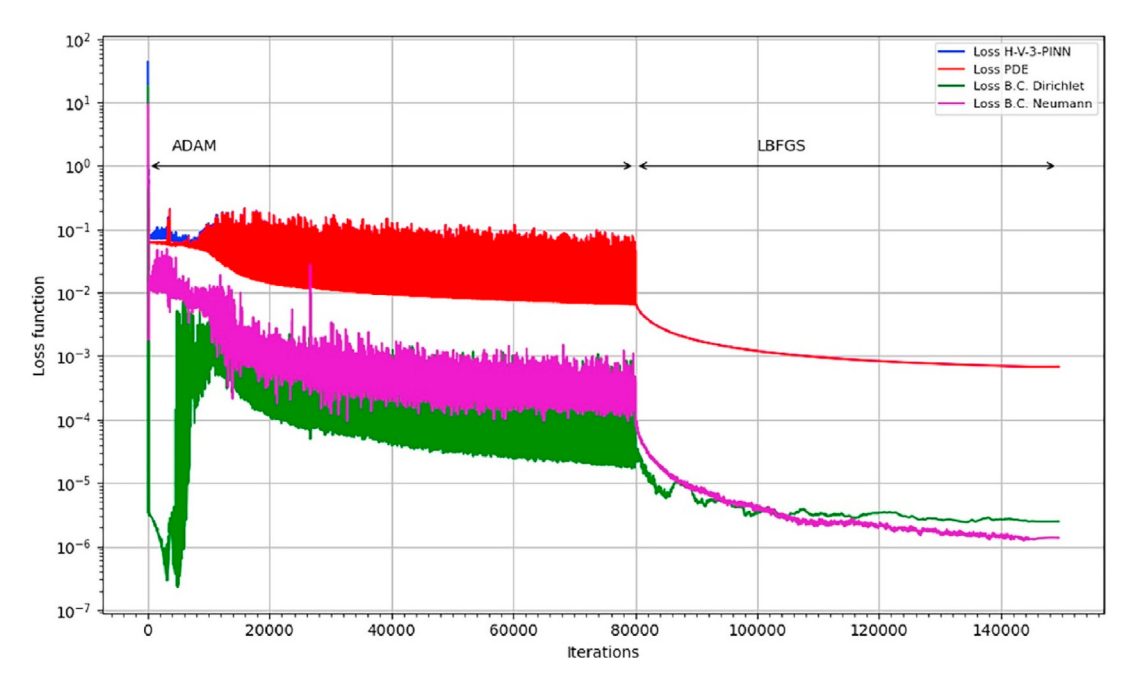


Fig. 8. Loss convergence of mixed-form PINN, reprinted from Fig. 10 in Lehmann et al. (2023). Convergence of H-V-3-PINN in the case of bi-directional flow in a heterogeneous domain: Variation of the total loss function and corresponding sub-terms (i.e. governing equation and boundary conditions) with respect to the number of iterations. Loss H-PINN-K represents the total loss function. Loss-PDE, Loss B.C. Dirichlet, and Loss B.C. Neumann represent the contribution of the governing equation and the Dirichlet and Neumann boundary conditions, respectively.

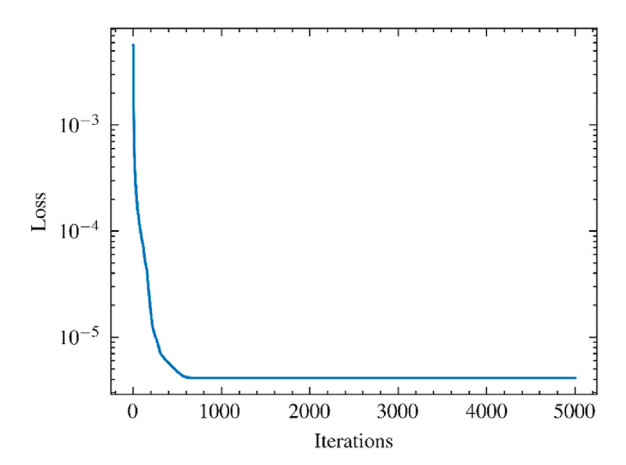


Fig. 9. PEFEN loss convergence of bi-directional flow in a heterogeneous domain.

should also be collected. The loss function contains multiple terms which are summarized as follows:

$$L = L_{\Omega} + \lambda_{D} L_{\partial \Omega_{D}} + \lambda_{N} L_{\partial \Omega_{N}}$$

$$L_{\Omega} = \frac{1}{N_{\Omega}} \sum_{i=1}^{N_{\Omega}} \left| \nabla \cdot \left[K(x_{\Omega_{i}}, y_{\Omega_{i}}) \nabla \widehat{H}(x_{\Omega_{i}}, y_{\Omega_{i}}) \right] \right|^{2}$$

$$L_{\partial \Omega_{D}} = \frac{1}{N_{\partial \Omega_{D}}} \sum_{i=1}^{N_{\partial \Omega_{D}}} \left| \widehat{H}(x_{\partial \Omega_{Di}}, y_{\partial \Omega_{Di}}) - g \right|^{2}$$

$$L_{\partial \Omega_{N}} = \frac{1}{N_{\partial \Omega_{N}}} \sum_{i=1}^{N_{\partial \Omega_{N}}} \left| \nabla \widehat{H}(x_{\partial \Omega_{Ni}}, y_{\partial \Omega_{Ni}}) \cdot n - h \right|^{2}$$
(9)

where the total loss L contains L_{Ω} (the PDE loss at interior collocation points), $L_{\partial\Omega_{\rm D}}$ (the loss at collocation points on Dirichlet

boundaries), and $L_{\partial\Omega_{\rm N}}$ (the loss at collocation points on Neumann boundaries). $L_{\partial\Omega_{\rm N}}$ and $L_{\partial\Omega_{\rm N}}$ can also include the loss of labeled data.

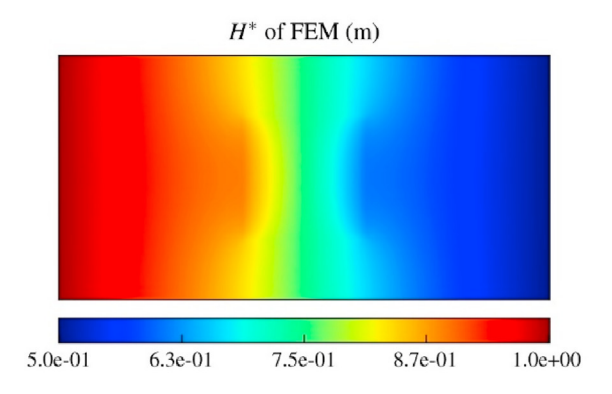
Automatic differentiation of neural networks can be leveraged to compute the derivatives in Eq. (3), in which second-order derivatives are required. If a heterogeneous domain should be considered, the function of hydraulic conductivity K(x,y) would be more complicated. The discontinuous heterogeneity leads to a discontinuous K(x,y), and the automatic differentiation probably fails (Lehmann et al., 2023). Conventional PINNs, thus, are confronted with prohibitive challenges in more practical cases where discontinuous heterogeneity is ubiquitous.

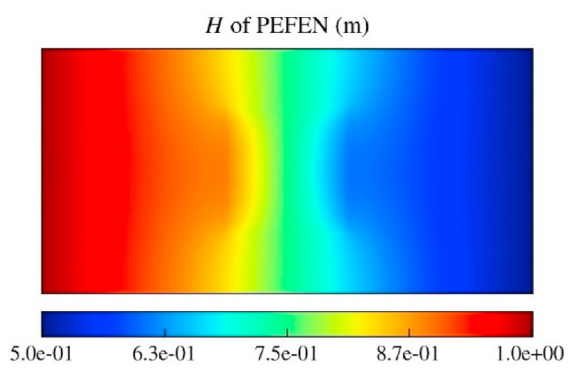
To demonstrate the failure mode of PINN, we utilize the published library of PINN named DeepXDE (Lu et al., 2021) to simulate a heterogeneous case as shown in Fig. 1a. The specific setting follows Lehmann et al. (2023). This PINN uses a neural network with three hidden layers, 56 neurons per hidden layer, two inputs for coordinates, and one output for hydraulic head. Fig. 1b presents the FEM reference result. This PINN converges as shown in Fig. 1f. Its result is depicted in Fig. 1c. The error distribution is shown in Fig. 1d. Given that the result is essentially one-dimensional, the hydraulic head along the horizontal cross-section is plotted in Fig. 1e. It shows that PINN cannot easily learn the sharp/steep gradients. Spectral bias or F-principle can explain this failure mode (Rahaman et al., 2019; Xu et al., 2020b). Local fluctuations caused by heterogeneity are more like high-frequency functions. However, conventional DNNs tend to learn low-frequency functions, which vary globally without local fluctuations as shown in Fig. 1e. Detailed discussions of using PEFEN on this case will be presented in Section

${\bf 3.} \ \ {\bf Methodology} \ \ {\bf of} \ \ {\bf the} \ \ {\bf physics-encoded} \ \ {\bf finite} \ \ {\bf element} \\ {\bf network} \\$

3.1. Functional losses

When the functional of a PDE exists, setting its first variation to





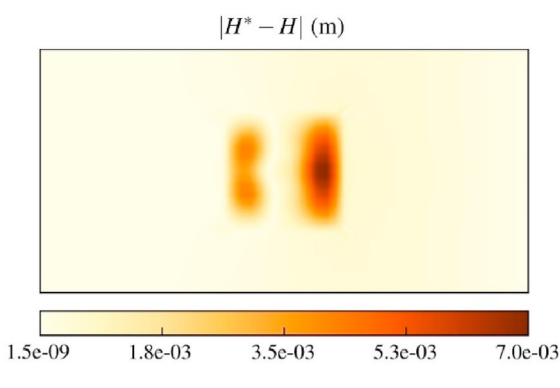


Fig. 10. Comparison of hydraulic head from FEM and PEFEN in the case of bidirectional flow in a heterogeneous domain.

zero is the first step to the strong form PDE as shown in Eq. (3) under certain Neumann boundary conditions in Eq. (4). The Dirichlet boundary condition in Eq. (5) is assumed to be satisfied in advance. The corresponding functional $\Pi(H)$ of Eqs. (3) and (4) is

$$\Pi(H) = \int_{\Omega} \frac{1}{2} K |\nabla H|^2 d\Omega - \int_{\partial \Omega_N} h \cdot H d\Gamma$$
 (10)

where the derivative order with respect to H is one, lower than the derivative order of two in Eq. (3).

3.2. PEFEN for porous flow

Fig. 2 gives an overview of the PEFEN for porous flow. The spatial domain is discretized by a structured or unstructured mesh that is composed of elements with no overlap. A standard nodal continuous finite element approximation is used to compute the hydraulic head at arbitrary points in the target domain. The hydraulic head H_0 at nodes is defined as both target variables and trainable

parameters. Since no labeled data are considered, H_0 will be initialized to zero at the outset.

For any point inside an element with $n_{\rm node}$ nodes $\{(x_1,y_1),(x_2,y_2),...,(x_{n_{\rm node}},y_{\rm node})\}$, the nodal basis functions are $\{l_1,l_2,...,l_{n_{\rm node}}\}$. The nodal hydraulic heads are $\{H_{01},H_{01},...,H_{0n_{\rm node}}\}$. The hydraulic head H at a point (x,y) inside the element is

$$H(x,y) = \sum_{i=1}^{n_{\text{node}}} l_i(x,y) H_{0i}$$
 (11)

At the point (x, y), the derivatives $\partial H/\partial x$ and $\partial H/\partial y$ can be calculated with the following linear operations on H_0 :

$$\frac{\partial H}{\partial x} = \sum_{i=1}^{n_{\text{node}}} \frac{\partial l_i(x, y)}{\partial x} H_{0i}
\frac{\partial H}{\partial y} = \sum_{i=1}^{n_{\text{node}}} \frac{\partial l_i(x, y)}{\partial y} H_{0i}$$
(12)

PEFEN can embody powerful nonlinearity even without DNNs. With respect to nodal H_0 , Eqs. (11) and (12) are linear transformations. Eqs. (11) and (12), and nodal H_0 of all discretized elements constitute the approximation function of hydraulic head H and its gradients $(\partial H/\partial x, \partial H/\partial y)$. The spatial nonlinearity of this approximation function originates from the basis functions $l_i(x,y)$. This study uses basis functions in quadratic serendipity elements. It circumvents the usage of nonlinear activation functions in DNNs. Combining nonlinear basis functions of connected finite elements, PEFEN can easily approximate highly nonlinear H.

As illustrated in Fig. 2a, after obtaining the hydraulic head and its derivatives with respect to x and y, the functional in Eq. (10) is encoded into the network. No additional labeled data are required. Neumann boundary conditions are naturally considered by its work. Dirichlet boundary conditions, as presented in Fig. 2b, can be strictly enforced by direct substitution. The hydraulic heads at these two nodes on $\partial\Omega_D$ are denoted H^1 and H^2 . The Dirichlet boundary value g directly substitutes these hydraulic heads like that in classical FEM (Zienkiewicz et al., 2005):

$$H^1 = H^2 = g (13)$$

Setting the node value will take effect by influencing its surrounding hydraulic heads H and gradients $(\partial H/\partial x, \partial H/\partial y)$ through Eqs. (11) and (12), thereby altering the final target minimum of the functional in Eq. (10). Since the loss function consists solely of a functional over the domain, the problem of imbalanced losses and gradient pathology can be alleviated in PEFEN.

The PEFEN in Fig. 2 is implemented in mainstream deep learning frameworks as a differentiable computational graph. Like the strategy in PINN, the problem can be solved by minimizing the scalar functional energy. In contrast to blackbox DNNs, the differentiable network in Fig. 2a is fully interpretable. If we aim to solve PDEs for other problems, a similar computational graph can be readily established like that in Fig. 2a. Operations to compute the loss for a different PDE can substitute the computational graph after getting $(H, \partial H/\partial x, \partial H/\partial y)$. Moreover, we do not need to set the number of layers and the number of neurons in each layer like that in DNNs. These hyperparameters often necessitate intuitive trialand-error procedures. Guan (2024) suggested sparse neural networks for carbon neutrality. PEFEN can be viewed as a sparse neural network, and it can significantly reduce the number of iterations to contribute to low-carbon AI for science. Its superior performance will be validated in the subsequent numerical experiments.

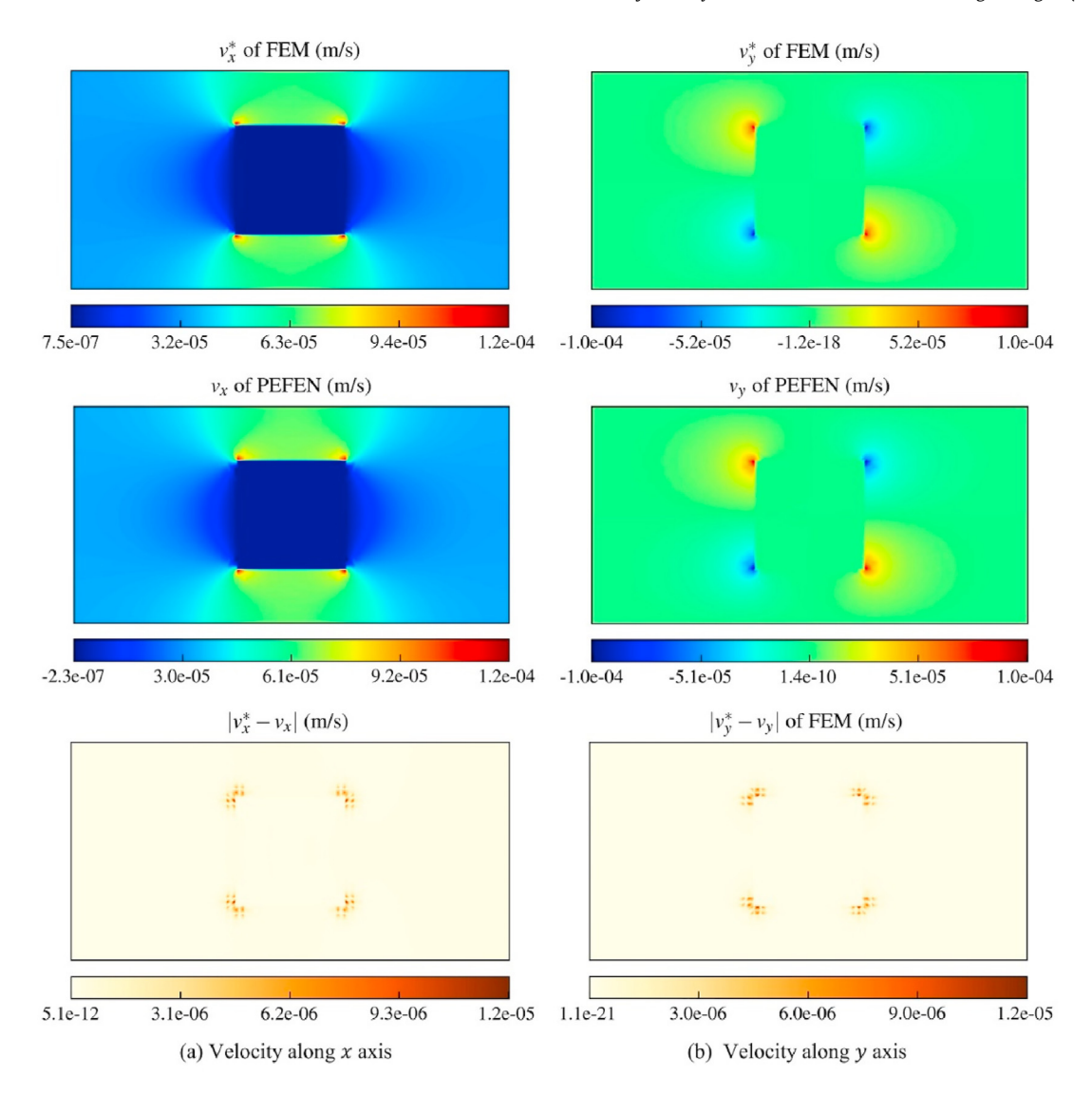


Fig. 11. Comparison of Darcy velocity from FEM and PEFEN in the case of bi-directional flow in a heterogeneous domain.

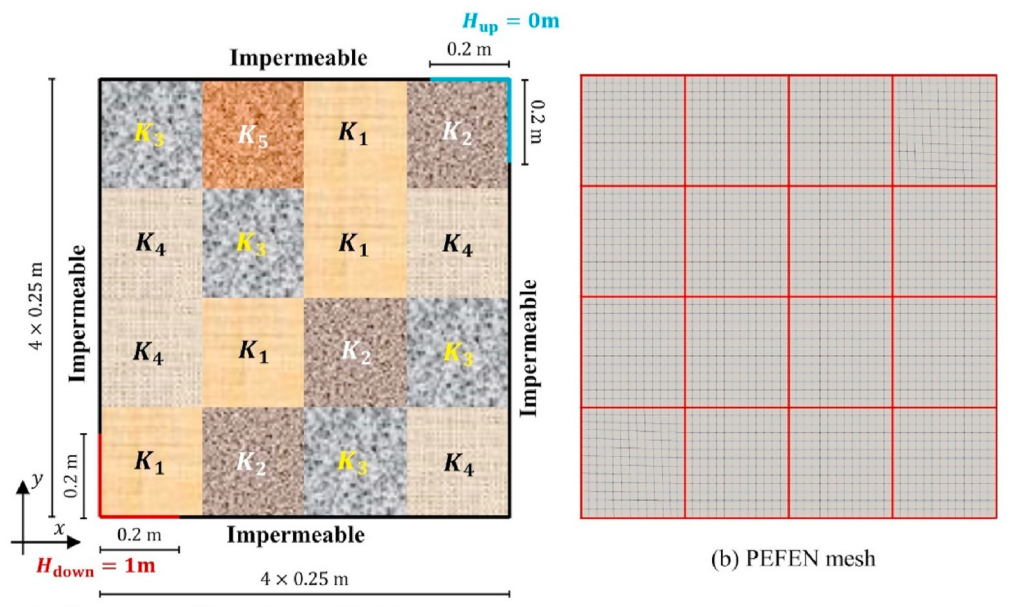
4. Numerical experiments

Lehmann et al. (2023) applied mixed-form PINN to solve heterogeneous flow problems and achieved satisfactory results. They utilized DNNs with three hidden layers and hyperbolic tangent activation functions. The hydraulic head and Darcy's velocity are directly output from single or multiple DNNs. More specific settings can be referred to in Lehmann et al. (2023). We reproduce the first three experiments from Lehmann et al. (2023) to validate the accuracy and much faster convergence of PEFEN. The last two cases are designed to address more practical geotechnical engineering problems, thereby showcasing the potential of PEFEN as an efficient differentiable forward solver.

The Adam optimizer (Kingma and Ba, 2017) and LBFGS optimizer (Liu and Nocedal, 1989) mentioned in this study refer to the implementation in PyTorch (refer to the PyTorch documentation for details on the LBFGS and Adam algorithms). The Adam optimizer is typically employed prior to LBFGS to avoid saddle points. Compared to conventional DNNs, PEFEN can be considered as a very sparse network with much smaller search space. Consequently, PEFEN can

converge rapidly to the target optimum with LBFGS only. This study utilizes CPU (Intel Core i9-14900KF) to train the PEFEN network. The hardware used in Lehmann et al. (2023) is a GPU (NVIDIA Quadro RTX 4000). The computational time and training time mentioned in the subsequent experiments refer to wall-clock time. Double-precision floating-point numbers are used.

The reference result vector is denoted as H^* , and the result vector obtained from PEFEN is denoted as H. The length of H^* or H is n that denotes the number of collocation points (in this study, n is the number of Gaussian points). Eq. (14) defines the relative L^2 and L^∞ error norm (Haghighat et al., 2021a). Assuming $(H^*-H)=(err_1, err_2,...,err_n)$, its L^2 norm $\|H^*-H\|_2$ is $(\sum_{i=1}^n err_i^2)^{1/2}$, i.e. this scalar measures the error vector over the domain in Euclidean space. L^∞ error norm $\|H^*-H\|_\infty$ is a scalar as $\max_i |err_i|$ that characterizes the maximum absolute error over the domain. The corresponding norm of H^* is used for nondimensionalization and scales the error norm. Thus, relative L^2 error norm denotes the average error. Relative L^∞ error norm indicates the maximum error.



(a) Geometry and boundaries of high heterogeneous domain with 16 regular blocks

Fig. 12. Configuration of high heterogeneous domain with 16 regular blocks.

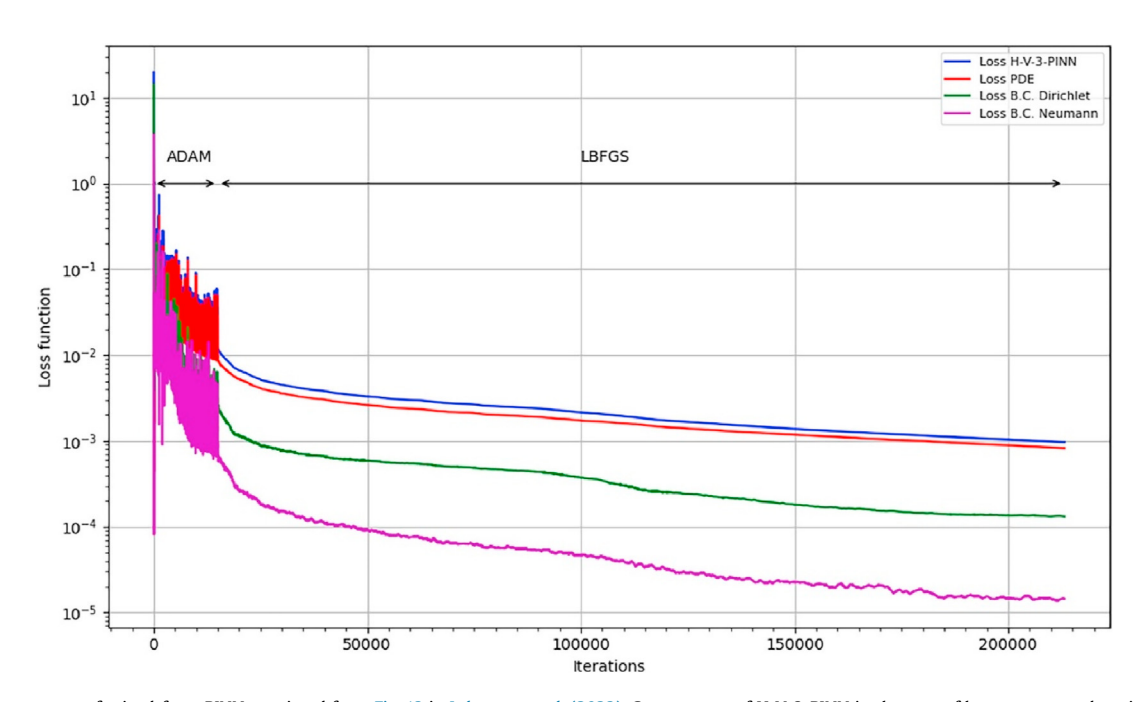


Fig. 13. Loss convergence of mixed-form PINN, reprinted from Fig. 13 in Lehmann et al. (2023). Convergence of H-V-3-PINN in the case of heterogeneous domain with 16 blocks: Variation of the total loss function and corresponding sub-terms (i.e. governing equation and boundary conditions) with respect to the number of iterations.

$$L^{2} \text{ relative error} = \frac{\|H^{*} - H\|_{2}}{\|H^{*}\|_{2}}$$

$$L^{\infty} \text{ relative error} = \frac{\|H^{*} - H\|_{\infty}}{\|H^{*}\|_{\infty}}$$
 (14)

4.1. Unidirectional flow in a heterogeneous domain

Fig. 3 presents the configuration of unidirectional flow in a heterogeneous domain. Fig. 3a illustrates the geometry and boundary conditions. The hydraulic head on the left is fixed as $H_{\text{left}}=1$ m, and the hydraulic head on the right is fixed as $H_{\text{right}}=0$ m. The upper and lower boundaries are impermeable. This domain is heterogeneous with a more permeable band in the middle right. The hydraulic conductivities are $K_1=1\times 10^{-4}$ m/s and $K_2=1\times 10^{-3}$ m/s. Fig. 3b displays the mesh in PEFEN and

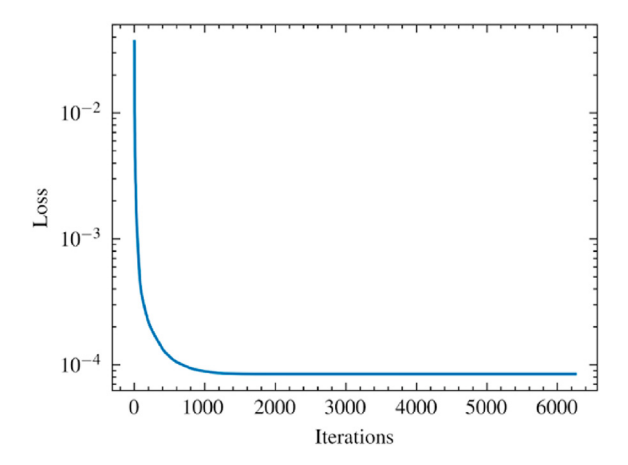


Fig. 14. PEFEN loss convergence of high heterogeneous domain with 16 regular blocks.

FEM, containing 128 quadratic serendipity elements. The fluid flow in this case will be unidirectional, and the velocity direction is towards the right. This case shares the same setting as those in Lehmann et al. (2023), and it was reported that the conventional PINN provided incoherent results due to discontinuity of the hydraulic conductivity. We have also discussed the failure mode of the conventional PINN in Section 2.

Thus, mixed-form PINN was proposed to solve the heterogeneous problem (Lehmann et al., 2023). Fig. 4 reprints the loss convergence of mixed-form PINN, in which 15,000 Adam iterations and about 15,000 LBFGS iterations are consumed. Its training time is about 10 min (600 s). In comparison, Fig. 5 illustrates the loss convergence of the PEFEN. It converges in just 400 LBFGS iterations, and only 0.5 s are consumed. It can be concluded that PEFEN converges much faster than the mixed-form PINN (400 iterations vs. 30,000 iterations, 0.5 s vs. 600 s).

Comparison between PEFEN and FEM are elaborated in Fig. 6. The hydraulic heads predicted by PEFEN align closely with reference FEM results. The relative L^2 error norm of hydraulic head is 1.03×10^{-4} , and the relative L^∞ error norm of hydraulic head is 2.62×10^{-4} . For Darcy velocity, relative L^2 error norm is 2.25×10^{-3} , and relative L^∞ error norm is 6.86×10^{-3} . To conclude, PEFEN can efficiently handle this heterogeneous case that the conventional PINN fails.

4.2. Bi-directional flow in a heterogeneous domain

Fig. 7 presents the configuration of bi-directional flow in a heterogeneous porous domain. Fig. 7a gives the geometry and boundaries. The hydraulic head on the left is fixed as $H_{\rm left}=1$ m, and the hydraulic head on the right is assigned as $H_{\rm right}=0$ m. The upper and lower boundaries are impermeable. A block with significantly lower hydraulic conductivity than the surrounding porous media is located in the middle, with much lower hydraulic conductivity than surrounding porous media, i.e. $K_1=9\times 10^{-5}$ m/s and $K_2=1\times 10^{-6}$ m/s. Fig. 7b shows the mesh in PEFEN and FEM, in which 1377 quadratic serendipity elements are discretized. The conventional PINN also failed in this case. Thus, He et al. (2020) used a DNN to approximate the discontinuous hydraulic conductivity field with a smoother one. Lehmann et al. (2023) adopted the mixed-form PINN for a better reproduction of the discontinuous heterogeneity.

Fig. 8 reprints the loss convergence of the mixed-form PINN. It took 80,000 Adam iterations and about 70,000 LBFGS iterations to reach the correct solution. About 2 h (7200 s) of computation time was consumed. In comparison, as shown in Fig. 9, PEFEN only spent

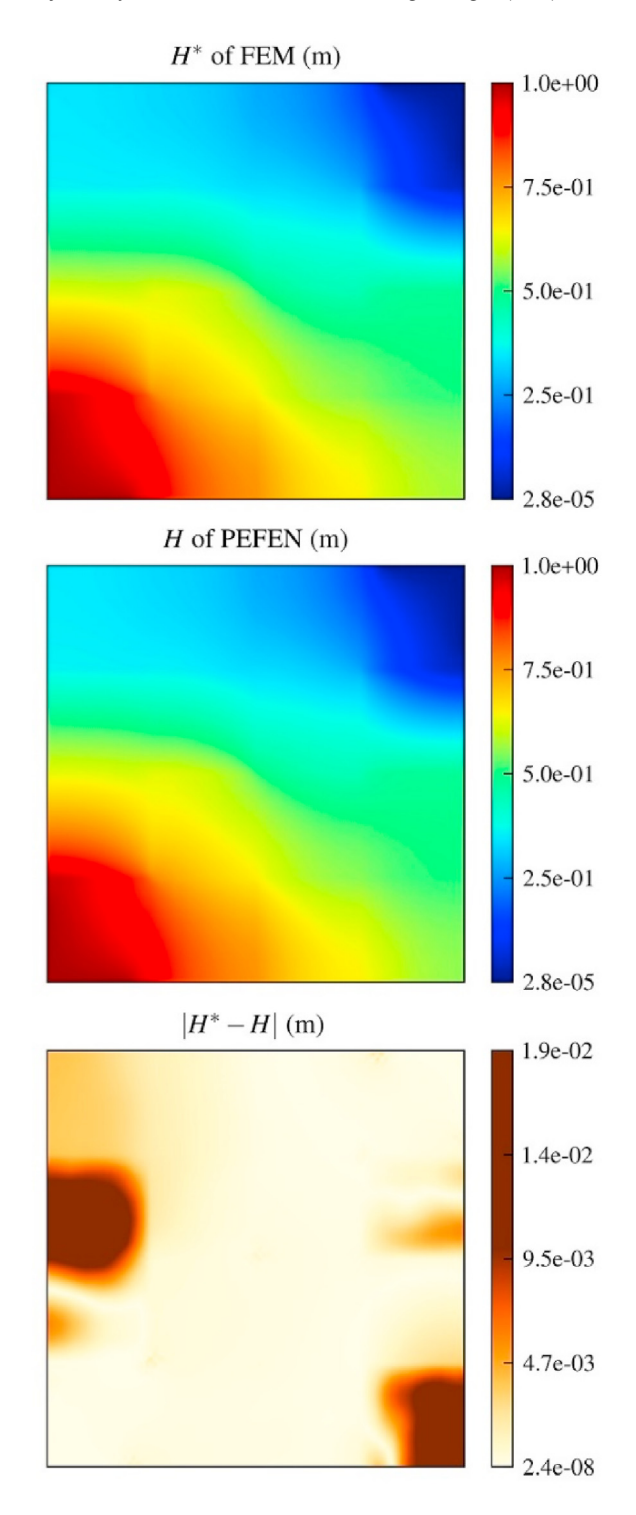


Fig. 15. Comparison of hydraulic head from FEM and PEFEN in the case of high heterogeneous domain with 16 regular blocks.

5000 LBFGS iterations and 17 s to reach convergence. It can be concluded that PEFEN converges much faster than the mixed-form PINN (5000 iterations vs. 150,000 iterations, 17 s vs. 7200 s).

Fig. 10 compares the hydraulic head from PEFEN and FEM. PEFEN gives the same pattern as FEM. The L^2 relative error of hydraulic head is 1.33×10^{-3} , and the L^{∞} relative error of hydraulic head is 7.05×10^{-3} . The largest error is about 7.05×10^{-3} . For mixed-form PINN, the largest error is about 1.2×10^{-2} in the same

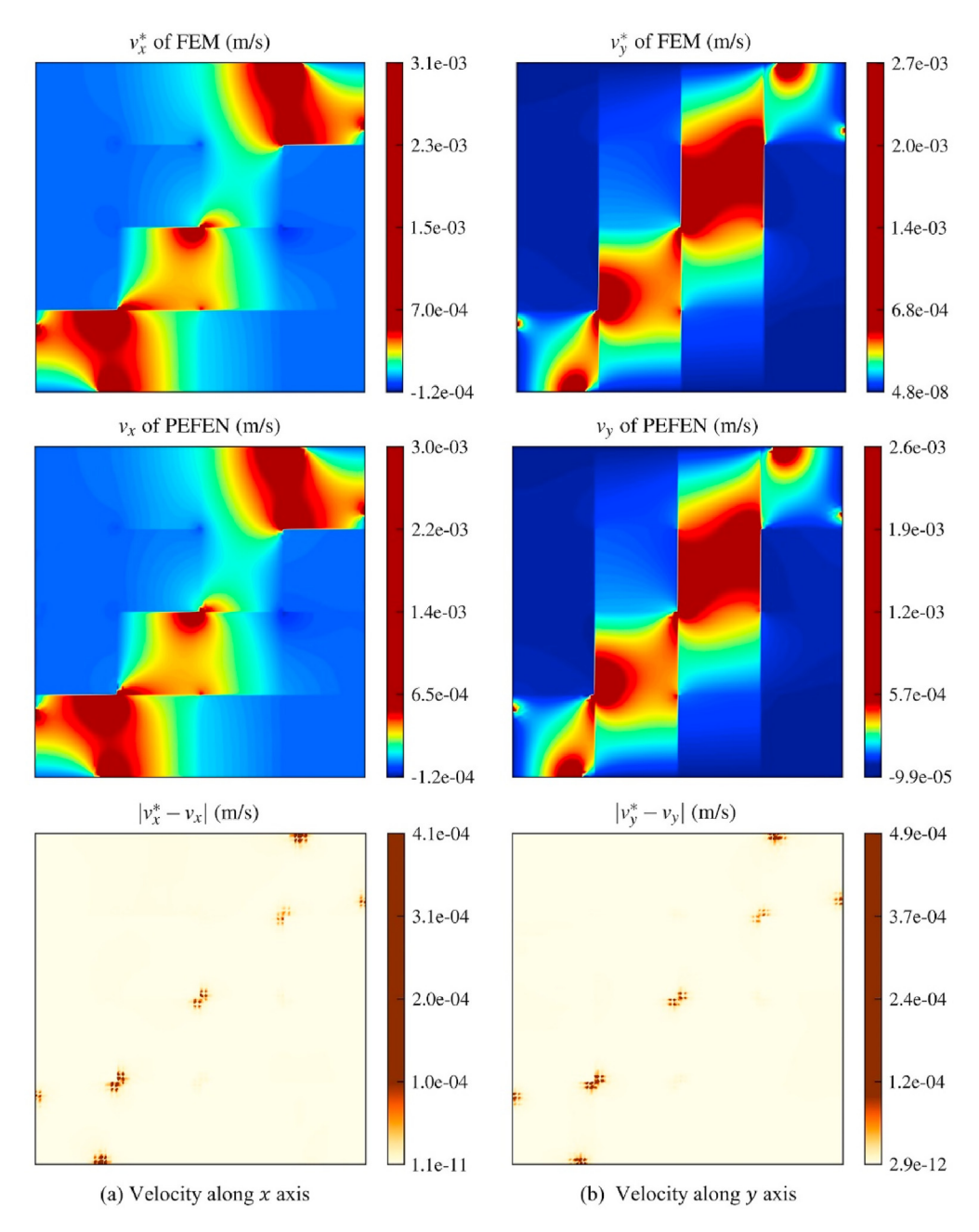


Fig. 16. Comparison of Darcy velocity from FEM and PEFEN in the case of high heterogeneous domain with 16 regular blocks.

case (Lehmann et al., 2023). The largest error occurs around the middle block with low hydraulic conductivity. Therefore, PEFEN can compute the hydraulic head in this heterogeneous case with high accuracy. Note that Fig. 9 presents quite a long plateau, during which relative errors do not reduce much. After 1000 iterations, the L^2 relative error of hydraulic head is 2.49×10^{-3} , and the L^∞ relative error of hydraulic head is 1.22×10^{-2} . The largest error is about 1.22×10^{-2} , which is quite close to the largest error of 1.2×10^{-2} in the same case of mixed-form PINN (Lehmann et al., 2023). Thus, the efficiency of PEFEN can be more promising if we only want to reach the same accuracy as mixed PINN (1000 iterations vs. 150,000 iterations, 7 s vs. 7200 s). The plateau exists because the default convergence criterion of LBFGS in PyTorch is strict.

The previous mixed-form PINN did not give detailed quantitative analysis of Darcy velocity (Lehmann et al., 2023). This study

presents the Darcy velocity along x-axis and y-axis in Fig. 11. PEFEN can reproduce the velocity pattern with high accuracy. The L^2 relative errors of v_x and v_y are 1.25×10^{-2} and 5.87×10^{-2} . The average relative error is relatively low. The largest error occurs around the discontinuous material interface. The L^∞ relative errors of v_x and v_y are 9.90×10^{-2} and 1.15×10^{-1} . Due to the discontinuous hydraulic conductivity, the maximum error is larger than the average error, but the predicted pattern is not influenced.

4.3. Highly heterogeneous domain with 16 regular blocks

Fig. 12 presents the highly heterogeneous case. There are 16 discontinuous heterogeneous blocks, which emulate the zonation techniques used for the identification of heterogeneous domains (Lehmann et al., 2023). The lower left corner is assigned the

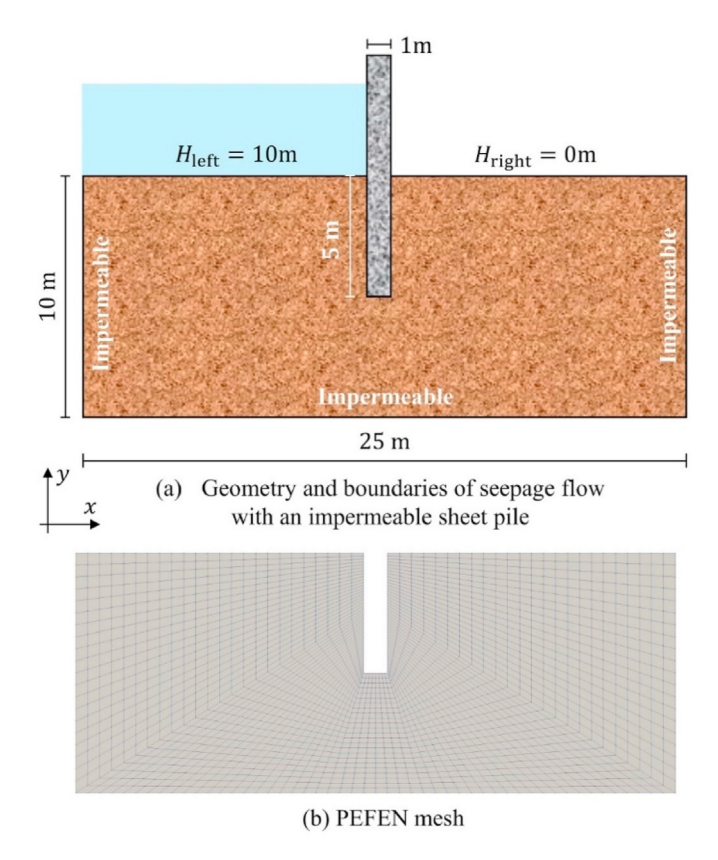


Fig. 17. Configuration of seepage flow with an impermeable sheet pile.

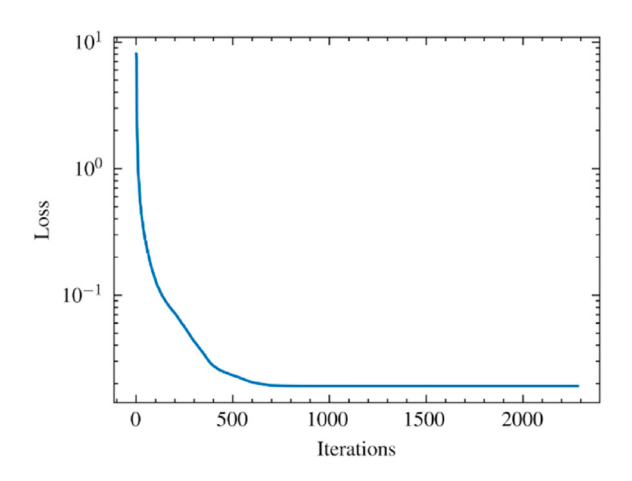


Fig. 18. PEFEN loss convergence of seepage flow with an impermeable sheet pile.

hydraulic head $H_{\rm down}=1$ m, and the upper right corner is assigned the hydraulic head $H_{\rm up}=0$ m. The remaining boundaries are impermeable. Hydraulic conductivities in different blocks are: $K_1=9\times 10^{-4}$ m/s, $K_2=5\times 10^{-4}$ m/s, $K_3=1\times 10^{-4}$ m/s, $K_4=1\times 10^{-5}$ m/s, $K_5=3\times 10^{-4}$ m/s. The mesh used in PEFEN and FEM contains 2704 quadratic serendipity elements.

Fig. 13 reprints the loss convergence of the mixed-form PINN. About 10,000 Adam iterations and 200,000 LBFGS iterations are entailed to reach the correct solution, which consumes 5 h (18,000 s). PEFEN loss in Fig. 14 reaches convergence in about 6000 iterations. PEFEN only takes 32 s. Thus, PEFEN demonstrates significantly greater efficiency than the improved mixed-form PINN (6000 iterations vs. 210,000 iterations, 32 s vs. 18,000 s).

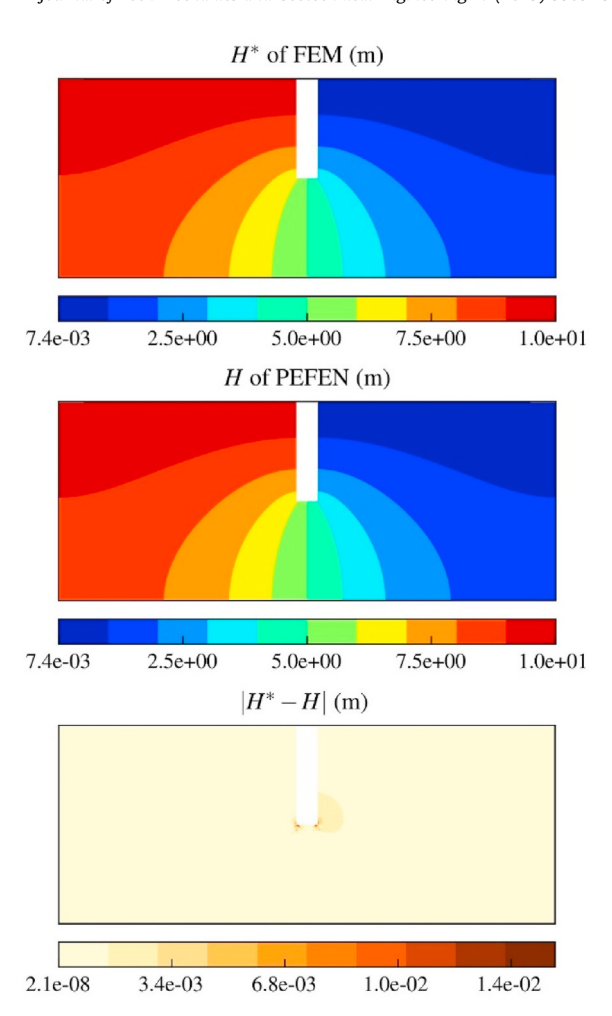


Fig. 19. Comparison of hydraulic heads from FEM and PEFEN in the case of seepage flow with an impermeable sheet pile.

Figs. 15 and 16 compare the hydraulic head and Darcy velocity between PEFEN and FEM. The resulting pattern from PEFEN is almost identical to FEM. The relative L^2 error norm of hydraulic head is 7.12×10^{-3} , and the relative L^∞ error norm of hydraulic head is 1.92×10^{-2} . The largest error is approximately 1.9×10^{-2} . For mixed-form PINN, the largest error is about 4.0×10^{-2} in the same case (Lehmann et al., 2023). L^2 relative errors of v_x and v_y are 4.44×10^{-2} and 4.08×10^{-2} . The average relative error is quite low. The largest error occurs around the discontinuous material interface. The relative L^∞ error norms of v_x and v_y are 1.3×10^{-1} and 1.8×10^{-1} . Because of the discontinuous hydraulic conductivity, the maximum error is larger than the average error, but the predicted pattern is not influenced. The velocity error is concentrated around the neighboring domains of the discontinuous material interfaces.

4.4. Seepage flow with an impermeable sheet pile

This study focuses on a more practical setting in geotechnical engineering. Fig. 17 presents the configuration of seepage flow with an impermeable sheet pile. The hydraulic head on the left is $H_{\rm left}=10$ m, and the hydraulic head on the right is $H_{\rm left}=0$ m. An impermeable sheet pile is inserted in the middle to mitigate seepage. The stratum in this case is homogeneous, with a hydraulic conductivity 9×10^{-4} m/s. Fig. 17b shows the mesh used in PEFEN and FEM, containing 2160 quadratic serendipity elements.

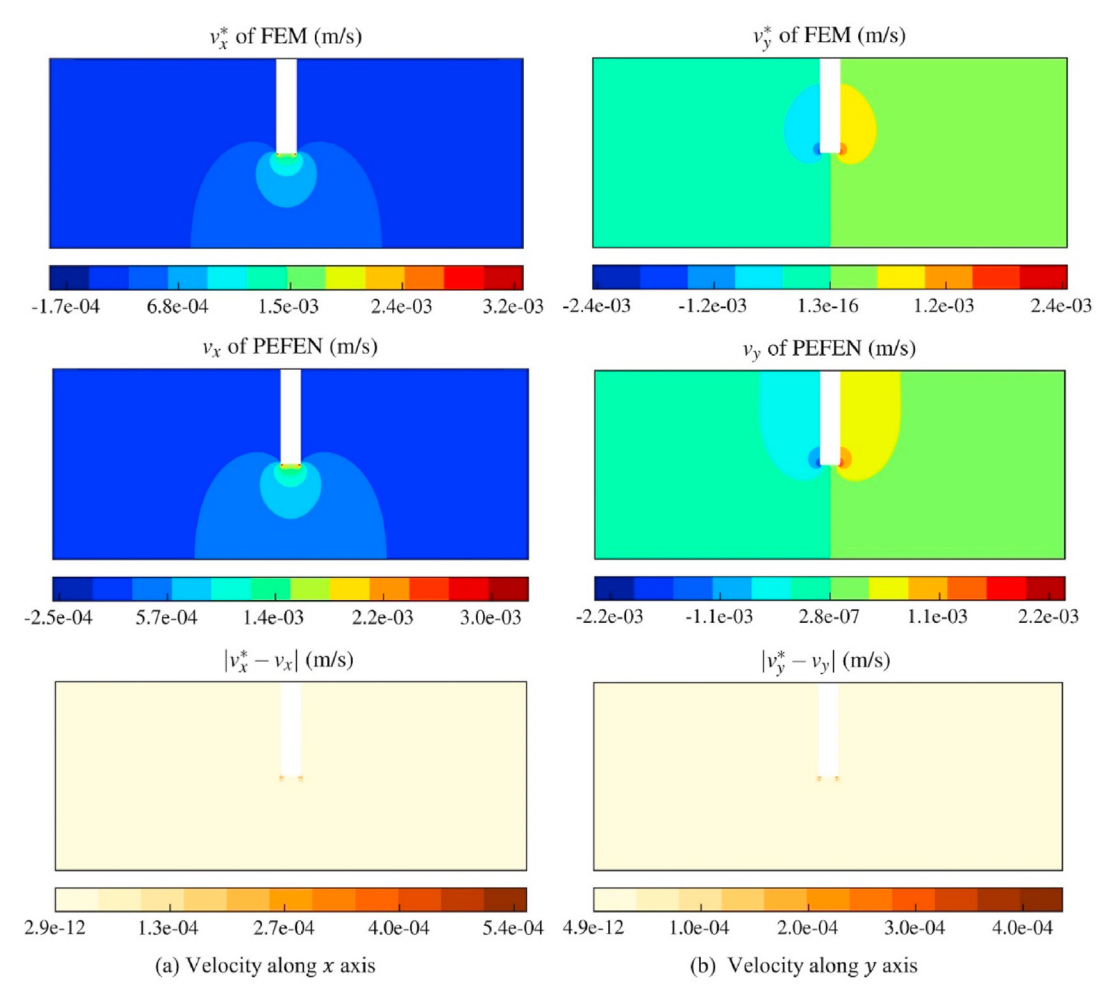


Fig. 20. Comparison of Darcy velocity from FEM and PEFEN in the case of seepage flow with an impermeable sheet pile.

Fig. 18 presents the loss convergence. PEFEN converges in 2500 LBFGS iterations, which takes 8.2 s. The hydraulic head in Fig. 19 validates the accuracy of PEFEN. Relative L^2 error norm of hydraulic head is 1.49×10^{-4} , and relative L^{∞} error norm of hydraulic head is 1.37×10^{-3} . The maximum error is larger than the average error because of the heterogeneity brought by an impermeable sheet pile. Fig. 20 gives the comparison of Darcy velocity components. PEFEN can accurately reproduce the pattern of velocities. The average error is small. Relative L^2 error norms of v_x and v_y are 3.44× 10^{-2} and 2.34×10^{-2} . The largest error occurs around the discontinuous material interface. Relative L^{∞} error norms of v_x and $v_{\rm V}$ are 1.65×10^{-1} and 1.65×10^{-1} . Because of the discontinuous hydraulic conductivity, the maximum error is larger than average error, but the predicted pattern is the same with FEM. The velocity error is concentrated in the neighboring domains of the discontinuous material interfaces.

4.5. Seepage flow in multi-layer strata with an impermeable sheet pile

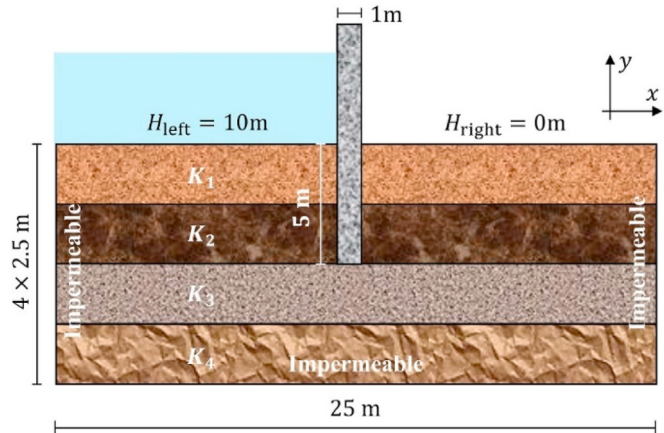
The former case studies the homogeneous stratum with an impermeable sheet pile. This case advances further toward practical geotechnical engineering, by considering multi-layer strata with discontinuous heterogeneity. Fig. 21 presents the configuration, which consists of four different layers. The hydraulic conductivities are as follows: $K_1 = 9 \times 10^{-4} \text{m/s}$, $K_2 = 5 \times 10^{-4} \text{m/s}$, s,

 $K_3=1\times 10^{-4} {\rm m/s}$, $K_4=1\times 10^{-5} {\rm m/s}$. Fig. 21b shows the mesh in PEFEN and FEM. There are 3920 quadratic serendipity elements. Fig. 22 presents the loss convergence of PEFEN. It converges in 3200 LBFGS iterations, and the wall-clock time is 28 s.

Fig. 23 presents the hydraulic head of PEFEN and FEM. Compared with the hydraulic head of homogeneous stratum in Fig. 19, the results of heterogeneous strata in Fig. 23 are very different. Relative L^2 error norm of hydraulic head is 1.45×10^{-3} , and relative L^{∞} error norm of hydraulic head is 5.31 \times 10⁻³. PEFEN demonstrates high accuracy in reproducing the hydraulic head. Fig. 24 presents the Darcy velocity, and v_x is significantly influenced by discontinuous heterogeneity. Errors of v_X and v_V concentrate around the bottom of the sheet pile. The average error is small. Relative L^2 error norms of v_X and v_Y are 5.75×10^{-2} and $4.42 \times$ 10^{-2} . The largest error occurs around the discontinuous material interface. Relative L^{∞} error norms of ν_x and ν_y are 1.87×10^{-1} and 1.17×10^{-1} . Due to the discontinuous hydraulic conductivity, the maximum error is larger than the average error, but the predicted pattern is the same with FEM. The velocity error is concentrated around the neighboring domains of the discontinuous material interfaces.

5. Discussion

The failure mode of conventional PINN is illustrated in Fig. 1. It fails probably because conventional DNNs struggle to adapt to local



(a) Geometry and boundaries of seepage flow in multi-layer strata with an impermeable sheet pile

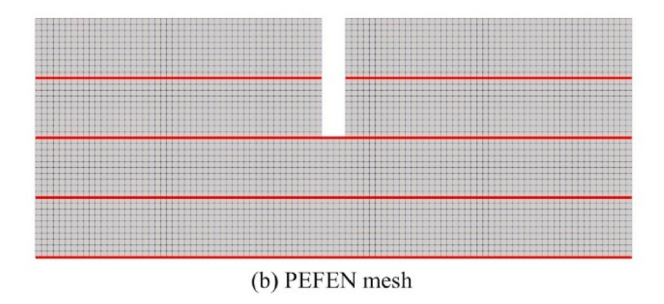


Fig. 21. Configuration of seepage flow with an impermeable sheet pile.

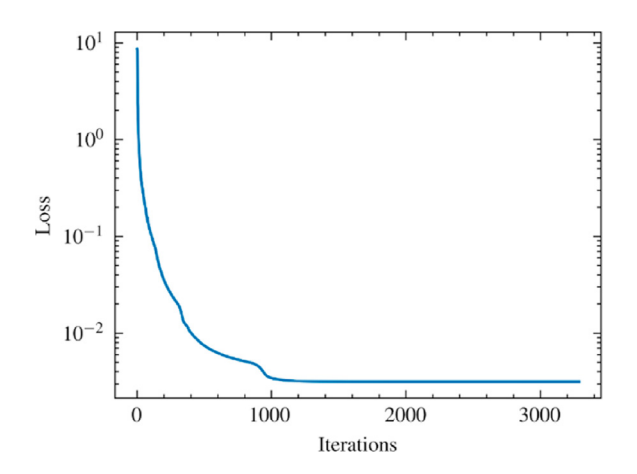


Fig. 22. PEFEN loss convergence of seepage flow in multi-layer strata with an impermeable sheet pile.

fluctuations with steep/sharp gradients that feature high-frequency functions (Rahaman et al., 2019; Xu et al., 2020b). Moreover, automatic differentiation cannot handle discontinuous parameters without proper approximation and special treatments. In contrast, PEFEN proves capable of solving complex heterogeneous problems without labeled data or special treatment. Reasons can be twofold: finite element decomposition and nonlinear approximation without activation functions. The heterogeneous domain is decomposed into discretized finite elements, decomposing the global heterogeneity to local homogeneity. It is much easier to approximate simple functions on decomposed elements, and thus PEFEN can solve discontinuous heterogeneity easily. On the other hand, Xu et al. (2020b) illustrated that the spectral bias

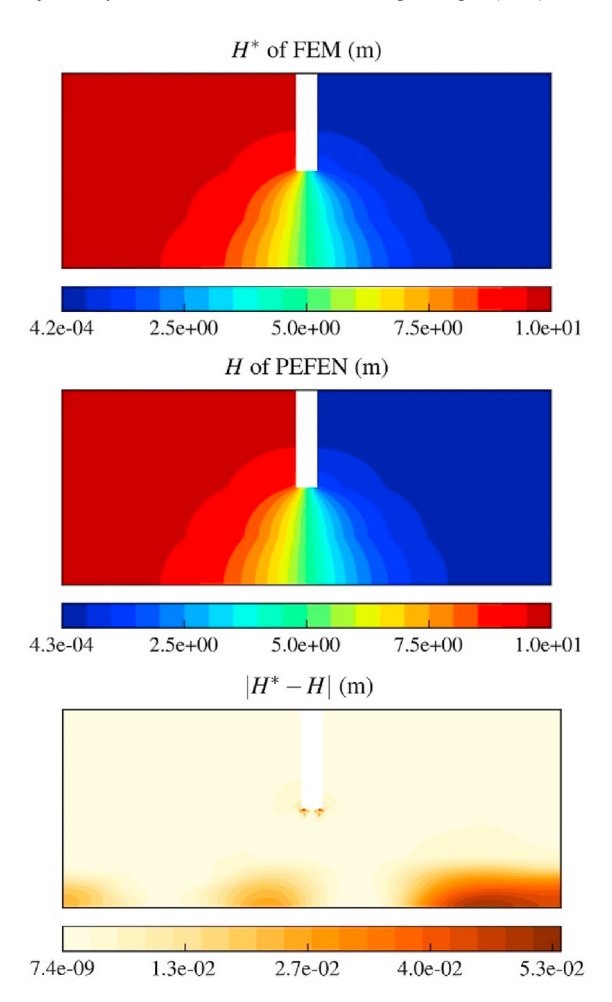


Fig. 23. Comparison of hydraulic head from FEM and PEFEN in the case of seepage flow in multi-layer strata with an impermeable sheet pile.

results from the smoothness/regularity of commonly used activation functions. In PEFEN, the finite element approximation can accurately fit complex functions of field variables without activation functions. Consequently, PEFEN, as a sparse network, can avoid the need to learn the blackbox weights/bias and efficiently solve discontinuous heterogeneous problems.

6. Conclusions

Since conventional PINNs struggle to solve practical porous flow problems with discontinuous heterogeneity without labeled data, this study employs a novel PEFEN. PEFEN encodes the Darcy's law and continuity equation as a functional, including the Neumann boundary conditions. The Dirichlet boundary conditions are also encoded into the discretized network. Compared with the improved PINN (mixed form), PEFEN does not predict additional stress variables and does not require tuning of DNN structures.

Numerical experiments validate the superior performance of PEFEN. The first three experiments demonstrate that PEFEN can effectively handle the discontinuous heterogeneity where conventional PINN fails. PEFEN converges much faster than the mixed-form PINN. Extraordinary improvement of convergence rate is achieved. Less than 1/30 iterations are entailed in PEFEN. It is because PEFEN can be considered as a sparse discretized network that features a much smaller search space, contributing to low-carbon AI for science.

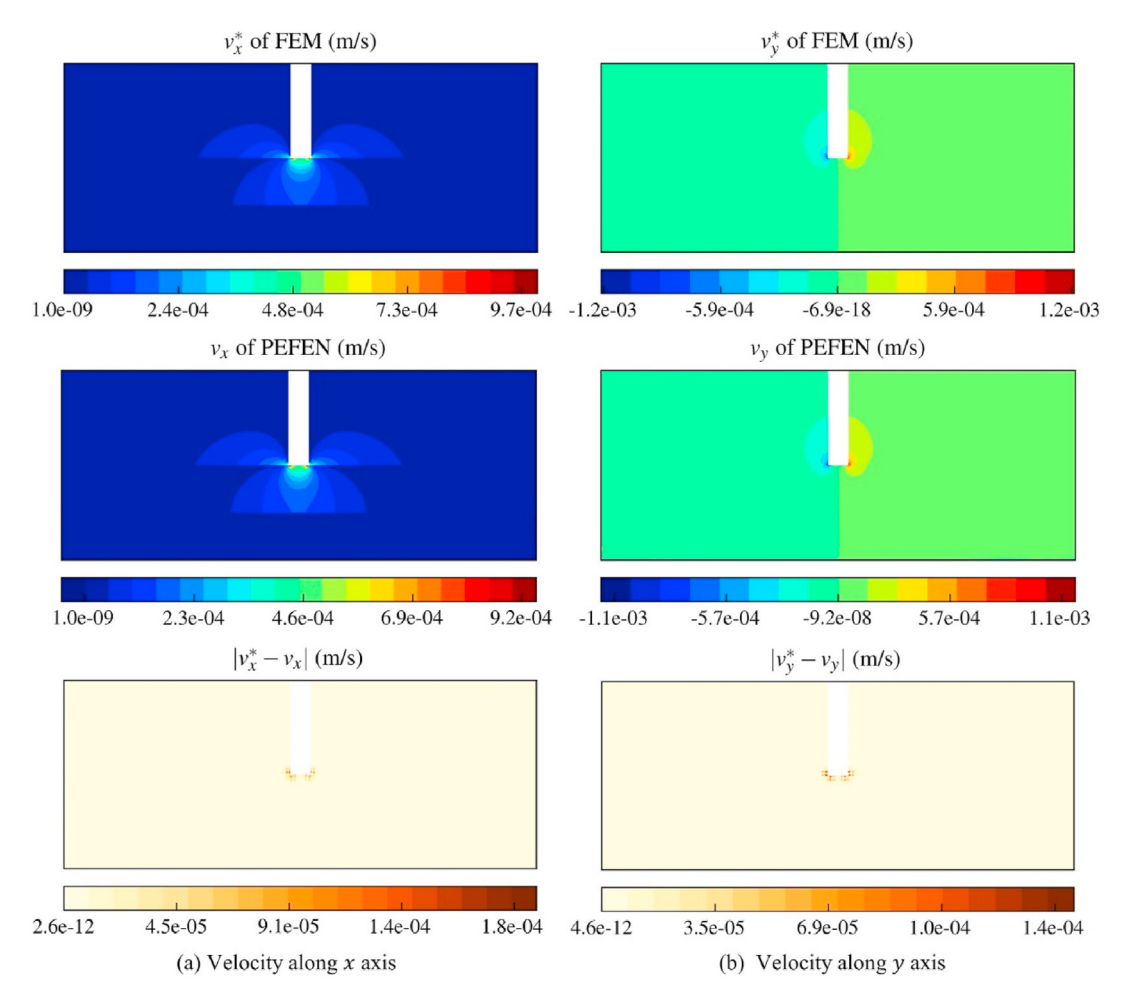


Fig. 24. Comparison of Darcy velocity from FEM and PEFEN in the case of seepage flow in multi-layer strata with an impermeable sheet pile.

The last two cases further corroborate PEFEN's capability for practical geotechnical studies. PEFEN proves to perform much better than PINN as an efficient forward solver for heterogeneous porous flow problems. Like PINNs, PEFEN solves problems by minimizing loss function that is flexible for different known and unknown parameters. Thus, PEFEN is promising for efficient forward and inverse analysis with limited labeled data, which is also our current research focus.

For future studies, we are working on PEFEN for more diverse applications on data assimilation and inverse analysis. This differentiable and physics-encoded way to combine PINN and traditional numerical methods proves quite promising. Further, it should be combined with operator learning or ensemble learning to build efficient surrogate models.

CRediT authorship contribution statement

Xi Wang: Writing — review & editing, Writing — original draft, Methodology, Formal analysis, Conceptualization. **Wei Wu:** Writing — review & editing, Supervision, Resources, Project administration, Funding acquisition. **He-Hua Zhu:** Writing — review & editing, Supervision, Resources, Funding acquisition.

Data availability statement

The PINN code is hosted at https://github.com/xiwang0706/ Projects-of-xiwang/tree/main, and the PEFEN code will be released after publishing some relevant works.

Declaration of competing interest

The authors declare that they have no known competing financial interests or personal relationships that could have appeared to influence the work reported in this paper.

Acknowledgments

This work was supported by the National Natural Science Foundation of China (Grant Nos. 42272338 and 41827807), and Department of Transportation of Zhejiang Province, China (Grant No. 202213). We would like to thank Professor Marwan Fahs, for his guidance about the basic knowledge of porous flow, the inspiration, and information of their published work.

References

Abueidda, D.W., Lu, Q., Koric, S., 2021. Meshless physics-informed deep learning method for three-dimensional solid mechanics. Int. J. Numer. Methods Eng. 122, 7182–7201.

Almajid, M.M., Abu-Al-Saud, M.O., 2022. Prediction of porous media fluid flow using physics informed neural networks. J. Pet. Sci. Eng. 208, 109205.

Bai, J., Rabczuk, T., Gupta, A., Alzubaidi, L., Gu, Y., 2023. A physics-informed neural network technique based on a modified loss function for computational 2D and 3D solid mechanics. Comput. Mech. 71, 543–562.

Bandai, T., Ghezzehei, T.A., 2022. Forward and inverse modeling of water flow in unsaturated soils with discontinuous hydraulic conductivities using physics-

- informed neural networks with domain decomposition. Hydrol. Earth Syst. Sci. 26, 4469—4495
- Bandai, T., Ghezzehei, T.A., 2021. Physics-informed neural networks with monotonicity constraints for richardson-richards equation: estimation of constitutive relationships and soil water flux density from volumetric water content measurements. Water Resour. Res. 57, e2020WR027642.
- Chen, X.-X., Zhang, P., Yin, Z.-Y., 2024. Physics-Informed neural network solver for numerical analysis in geoengineering. Georisk 0, 1–19.
- Diao, Y., Yang, J., Zhang, Y., Zhang, D., Du, Y., 2023. Solving multi-material problems in solid mechanics using physics-informed neural networks based on domain decomposition technology. Comput. Methods Appl. Mech. Eng. 413, 116120.
- Elkhadrawi, M., Ng. C., Bain, D.J., Sargent, E.E., Stearsman, E.V., Gray, K.A., Akcakaya, M., 2024. Novel physics informed-neural networks for estimation of hydraulic conductivity of green infrastructure as a performance metric by solving Richards—Richardson PDE. Neural Comput. Appl. 36, 5555—5569.
- Forsythe, G.E., Wasow, W.R., 1960. Finite-difference methods for partial differential equations. Appl. Mathemat. Ser.
- Gao, H., Zahr, M.J., Wang, J.-X., 2022. Physics-informed graph neural Galerkin networks: a unified framework for solving PDE-governed forward and inverse problems. Comput. Methods Appl. Mech. Eng. 390, 114502.
- Guan, L., 2024. Reaching carbon neutrality requires energy-efficient training of Al. Nature 626, 33. https://doi.org/10.1038/d41586-024-00200-x, 33.
- Guo, Q., Zhao, Y., Lu, C., Luo, J., 2023. High-dimensional inverse modeling of hydraulic tomography by physics informed neural network (HT-PINN). J. Hydrol. 616, 128828.
- Haghighat, E., Amini, D., Juanes, R., 2022. Physics-informed neural network simulation of multiphase poroelasticity using stress-split sequential training. Comput. Methods Appl. Mech. Eng. 397, 115141.
- Haghighat, E., Bekar, A.C., Madenci, E., Juanes, R., 2021a. A nonlocal physicsinformed deep learning framework using the peridynamic differential operator. Comput. Methods Appl. Mech. Eng. 385, 114012.
- Haghighat, E., Raissi, M., Moure, A., Gomez, H., Juanes, R., 2021b. A physics-informed deep learning framework for inversion and surrogate modeling in solid mechanics. Comput. Methods Appl. Mech. Eng. 379, 113741.
- Hanna, J.M., Aguado, J.V., Comas-Cardona, S., Askri, R., Borzacchiello, D., 2022. Residual-based adaptivity for two-phase flow simulation in porous media using Physics-informed Neural Networks. Comput. Methods Appl. Mech. Eng. 396, 115100.
- He, Q., Barajas-Solano, D., Tartakovsky, G., Tartakovsky, A.M., 2020. Physics-informed neural networks for multiphysics data assimilation with application to subsurface transport. Adv. Water Resour. 141, 103610.
- Karniadakis, G.E., Kevrekidis, I.G., Lu, L., Perdikaris, P., Wang, S., Yang, L., 2021. Physics-informed machine learning. Nat. Rev. Phys. 3, 422–440.
- Kingma, D.P., Ba, J., 2017. Adam: A Method for Stochastic Optimization.
- Kreyenberg, P.J., Bauser, H.H., Roth, K., 2019. Velocity field estimation on density-driven solute transport with a convolutional neural network. Water Resour. Res. 55, 7275–7293.
- Krishnapriyan, A.S., Gholami, A., Zhe, S., Kirby, R.M., Mahoney, M.W., 2021. Characterizing possible failure modes in physics-informed neural networks. In: Ranzato, M., Beygelzimer, A., Dauphin, Y., Liang, P.S., Vaughan, J.W. (Eds.), AD-VANCES IN NEURAL INFORMATION PROCESSING SYSTEMS 34 (NEURIPS 2021), Advances in Neural Information Processing Systems. Presented at the 35th Conference on Neural Information Processing Systems (NeurIPS), Neural Information Processing Systems (NeurIPS), Neural Information Processing Systems (Nips). La Jolla.
- Laloy, E., Hérault, R., Jacques, D., Linde, N., 2018. Training-image based geostatistical inversion using a spatial generative adversarial neural network. Water Resour. Res. 54, 381–406.
- Lan, P., Su, J., Zhang, S., 2023. Surrogate modeling for unsaturated infiltration via the physics and equality-constrained artificial neural networks. J. Rock Mech. Geotech. Eng.
- Lehmann, F., Fahs, M., Alhubail, A., Hoteit, H., 2023. A mixed pressure-velocity formulation to model flow in heterogeneous porous media with physicsinformed neural networks. Adv. Water Resour. 181, 104564.
- Li, X.F., Li, H.B., Liu, L.W., Liu, Y.Q., Ju, M.H., Zhao, J., 2020a. Investigating the crack initiation and propagation mechanism in brittle rocks using grain-based finitediscrete element method. Int. J. Rock Mech. Min. Sci. 127, 104219.
- Li, A., Liu, Y., Dai, F., Liu, K., Wei, M., 2020b. Continuum analysis of the structurally controlled displacements for large-scale underground caverns in bedded rock masses. Tunn. Undergr. Space Technol. 97, 103288.
- Li, X.F., Li, H.B., Zhao, J., 2021. Transgranular fracturing of crystalline rocks and its influence on rock strengths: insights from a grain-scale continuum—discontinuum approach. Comput. Methods Appl. Mech. Eng. 373, 113462.
- Li, Y., Ni, P., Sun, L., Xia, Y., 2024. Finite element model-informed deep learning for equivalent force estimation and full-field response calculation. Mech. Syst. Signal Process. 206, 110892.
- Liang, W., He, K.-Y., Jin, Y.-F., Yin, Z.-Y., 2024. A gradient-smoothed material point method for reducing cell crossing noise in large deformation problems. Comput. Geotech. 169, 106169.
- Liang, W., Zhao, J., 2019. Multiscale modeling of large deformation in geomechanics. Int. J. Numer. Anal. Methods GeoMech. 43, 1080–1114.
- Liang, W., Zhao, J., Wu, H., Soga, K., 2023. Multiscale, multiphysics modeling of saturated granular materials in large deformation. Comput. Methods Appl. Mech. Eng. 405, 115871.
- Liu, D.C., Nocedal, J., 1989. On the limited memory BFGS method for large scale

- optimization. Math. Program. 45, 503-528.
- Lu, L., Meng, X., Mao, Z., Karniadakis, G.E., 2021. DeepXDE: a deep learning library for solving differential equations. SIAM Rev. 63, 208–228.
- Luo, L., Song, M., Zhong, H., He, T., Sun, L., 2024a. Hierarchical Bayesian model updating of a long-span arch bridge considering temperature and traffic loads. Mech. Syst. Signal Process. 210, 111152.
- Luo, L., Sun, L., Li, Y., Xia, Y., 2024b. Structural nonlinear boundary condition identification using a hybrid physics data-driven approach. Nonlinear Dynam.
- Mao, Z., Jagtap, A.D., Karniadakis, G.E., 2020. Physics-informed neural networks for high-speed flows. Comput. Methods Appl. Mech. Eng. 360, 112789.
- Mo, S., Zabaras, N., Shi, X., Wu, J., 2019a. Deep autoregressive neural networks for high-dimensional inverse problems in groundwater contaminant source identification. Water Resour. Res. 55, 3856—3881.
- Mo, S., Zhu, Y., Zabaras, N., Shi, X., Wu, J., 2019b. Deep convolutional encoder-decoder networks for uncertainty quantification of dynamic multiphase flow in heterogeneous media. Water Resour. Res. 55, 703–728.
- Qu, T., Zhao, J., Guan, S., Feng, Y., 2023. Data-driven multiscale modelling of granular materials via knowledge transfer and sharing. Int. J. Plast. 171, 103786.
- Rahaman, N., Baratin, A., Arpit, D., Draxler, F., Lin, M., Hamprecht, F., Bengio, Y., Courville, A., 2019. On the spectral bias of neural networks. In: Proceedings of the 36th International Conference on Machine Learning. Presented at the International Conference on Machine Learning, PMLR, pp. 5301–5310.
- Raissi, M., Perdikaris, P., Karniadakis, G.E., 2019. Physics-informed neural networks: a deep learning framework for solving forward and inverse problems involving nonlinear partial differential equations. J. Comput. Phys. 378, 686–707.
- Rajabi, M.M., Hajizadeh Javaran, M.R., Bah, A., Frey, G., Le Ber, F., Lehmann, F., Fahs, M., 2022. Analyzing the efficiency and robustness of deep convolutional neural networks for modeling natural convection in heterogeneous porous media. Int. J. Heat Mass Tran. 183, 122131.
- Rao, C., Ren, P., Wang, Q., Buyukozturk, O., Sun, H., Liu, Y., 2023. Encoding physics to learn reaction—diffusion processes. Nat. Mach. Intell. 5, 765—779.
- Ren, H., Zhuang, X., Rabczuk, T., 2017. Dual-horizon peridynamics: a stable solution to varying horizons. Comput. Methods Appl. Mech. Eng. 318, 762–782.
- Secci, D., A Godoy, V., Gómez-Hernández, J.J., 2024. Physics-Informed Neural Networks for solving transient unconfined groundwater flow. Comput. Geosci. 182, 105494
- Shi, G., 1992. Discontinuous deformation analysis: a new numerical model for the statics and dynamics of deformable block structures. Eng. Comput. 9, 157–168. Silling S.A. Lehoucg R.B. 2010. Peridynamic theory of solid mechanics. Adv. Appl.
- Silling, S.A., Lehoucq, R.B., 2010. Peridynamic theory of solid mechanics. Adv. Appl. Mech. 44, 73–168.
- Sun, J., Hu, L., Li, D., Sun, K., Yang, Z., 2022. Data-driven models for accurate groundwater level prediction and their practical significance in groundwater management. J. Hydrol. 608, 127630.
- Sun, L., Sun, H., Zhang, W., Li, Y., 2024. Hybrid monitoring methodology: a model-data integrated digital twin framework for structural health monitoring and full-field virtual sensing. Adv. Eng. Inf. 60, 102386.
- Sun, Y., Cheng, H., Zhang, S., Mohan, M.K., Ye, G., De Schutter, G., 2023. Prediction & optimization of alkali-activated concrete based on the random forest machine learning algorithm. Construct. Build. Mater. 385, 131519.
- Tang, M., Liu, Y., Durlofsky, L.J., 2021. Deep-learning-based surrogate flow modeling and geological parameterization for data assimilation in 3D subsurface flow. Comput. Methods Appl. Mech. Eng. 376, 113636.
- Tartakovsky, A.M., Marrero, C.O., Perdikaris, P., Tartakovsky, G.D., Barajas-Solano, D., 2020. Physics-informed deep neural networks for learning parameters and constitutive relationships in subsurface flow problems. Water Resour. Res. 56, e2019WR026731.
- Virupaksha, A.G., Nagel, T., Lehmann, F., Rajabi, M.M., Hoteit, H., Fahs, M., Le Ber, F., 2024. Modeling transient natural convection in heterogeneous porous media with Convolutional Neural Networks. Int. J. Heat Mass Tran. 222, 125149.
- Wang, L., Liu, G., Wang, G., Zhang, K., 2024. M-PINN: a mesh-based physics-informed neural network for linear elastic problems in solid mechanics. Int. J. Numer. Methods Eng. n/a, e7444.
- Wang, N., Zhang, D., Chang, H., Li, H., 2020. Deep learning of subsurface flow via theory-guided neural network. J. Hydrol. 584, 124700.
- Wang, S., Teng, Y., Perdikaris, P., 2021. Understanding and mitigating gradient flow pathologies in physics-informed neural networks. SIAM J. Sci. Comput. 43, A3055—A3081.
- Wang, X., Wu, W., Zhu, H., Lin, J.-S., Zhang, H., 2019. Contact detection between polygonal blocks based on a novel multi-cover system for discontinuous deformation analysis. Comput. Geotech. 111, 56–65.
- Wang, X., Wu, W., Zhu, H., Zhang, H., 2022. Three-dimensional discontinuous deformation analysis derived from the virtual work principle with a simplex integral on the boundary. Comput. Geotech. 146, 104710.
- Wang, X., Yin, Z.-Y., 2024. Interpretable physics-encoded finite element network to handle concentration features and multi-material heterogeneity in hyperelasticity. Comput. Methods Appl. Mech. Eng. 431, 117268.
- Wang, Z., Cudmani, R., Alfonso Peña Olarte, A., 2024. Tensor-based physics-encoded neural networks for modeling constitutive behavior of soil. Comput. Geotech. 170. 106173.
- Wei, M., Dai, F., Ji, Y., Wu, W., 2021. Effect of fluid pressure gradient on the factor of safety in rock stability analysis. Eng. Geol. 294, 106346.
- Wu, H., Fang, W.-Z., Kang, Q., Tao, W.-Q., Qiao, R., 2019. Predicting effective diffusivity of porous media from images by deep learning. Sci. Rep. 9, 20387.
- Xu, G., He, C., Chen, Z., 2019. Mechanical behavior of transversely isotropic rocks with non-continuous planar fabrics under compression tests. Comput. Geotech.

115, 103175.

- Xu, G., Gutierrez, M., He, C., Meng, W., 2020a. Discrete element modeling of transversely isotropic rocks with non-continuous planar fabrics under Brazilian test. Acta Geotech 15, 2277–2304.
- Xu, Z.-Q.J., Zhang, Y., Luo, T., Xiao, Y., Ma, Z., 2020b. Frequency principle: fourier analysis sheds light on deep neural networks. CiCP 28, 1746–1767.
 Yang, B., Leng, Z., Jiang, J., He, Z., Li, D., 2022. Recovery efficiency of the damaged
- Yang, B., Leng, Z., Jiang, J., He, Z., Li, D., 2022. Recovery efficiency of the damaged porous asphalt mixture with emulsion-based surface treatment: material optimization and performance verification. Construct. Build. Mater. 347, 128530.
- Yang, C., Zhu, F., Zhao, J., 2024a. Coupled total- and semi-Lagrangian peridynamics for modelling fluid-driven fracturing in solids. Comput. Methods Appl. Mech. Eng. 419, 116580.
- Yang, C., Zhu, F., Zhao, J., 2024b. A multi-horizon fully coupled thermo-mechanical peridynamics. J. Mech. Phys. Solid. 105758.
- Yang, J., Liu, X., Diao, Y., Chen, X., Hu, H., 2024c. Adaptive task decomposition physics-informed neural networks. Comput. Methods Appl. Mech. Eng. 418, 116561.
- Yeung, Y.-H., Barajas-Solano, D.A., Tartakovsky, A.M., 2022. Physics-informed machine learning method for large-scale data assimilation problems. Water Resour. Res. 58, e2021WR031023.
- Yu, J., Zhao, J., Liang, W., Zhao, S., 2024a. A semi-implicit material point method for coupled thermo-hydro-mechanical simulation of saturated porous media in large deformation. Comput. Methods Appl. Mech. Eng. 418, 116462.
- Yu, J., Zhao, J., Zhao, S., Liang, W., 2024b. Thermo-hydro-mechanical coupled material point method for modeling freezing and thawing of porous media. Int. J. Numer. Anal. Methods GeoMech. 48, 3308–3349.
- Numer. Anal. Methods GeoMech. 48, 3308—3349.
 Zhang, X., Zhu, Y., Wang, J., Ju, L., Qian, Y., Ye, M., Yang, J., 2022. GW-PINN: a deep learning algorithm for solving groundwater flow equations. Adv. Water Resour. 165. 104243.
- Zhang, Z., 2022. A physics-informed deep convolutional neural network for simulating and predicting transient Darcy flows in heterogeneous reservoirs without labeled data. J. Pet. Sci. Eng. 211, 110179.
- labeled data. J. Pet. Sci. Eng. 211, 110179.

 Zhang, Z., Yan, X., Liu, P., Zhang, K., Han, R., Wang, S., 2023. A physics-informed convolutional neural network for the simulation and prediction of two-phase Darcy flows in heterogeneous porous media. J. Comput. Phys. 477, 111919.
- Zhao, S., Chen, H., Zhao, J., 2024. A physical-information-flow-constrained temporal graph neural network-based simulator for granular materials. Comput. Methods Appl. Mech. Eng. 433, 117536.

- Zhu, Y., Zabaras, N., 2018. Bayesian deep convolutional encoder—decoder networks for surrogate modeling and uncertainty quantification. J. Comput. Phys. 366, 415–447.
- Zhuang, B., Arcaro, A., Gencturk, B., Ghanem, R., 2024. Machine learning-aided damage identification of mock-up spent nuclear fuel assemblies in a sealed dry storage canister. Eng. Appl. Artif. Intell. 128, 107484.
- Zienkiewicz, O.C., Taylor, R.L., Zhu, J.Z., 2005. The Finite Element Method: its Basis and Fundamentals. Elsevier.



Xi Wang obtained his bachelor's degree and PhD in Civil Engineering from Tongji University with Academician Hehua Zhu as supervisor and Professor Wei Wu as cosupervisor. He obtained his master's degree of Science in Computer Science in University of Texas at Austin. Xi is a postdoctoral fellow in Hong Kong University of Science and Technology and Hong Kong Polytechnic University. His research interests focus on physics-informed neural networks (PINNs) and discontinuous deformation analysis (DDA), with applications in the field of geotechnical engineering.



Wei Wu is a professor (associate) at the Department of Geotechnical Engineering of Tongji University, China. He received his PhD in Civil Engineering from Tongji University in 2016. He is the deputy secretary general of the Commission on Discontinuous Deformation Analysis of Geomechanics in Chinese Society for Rock Mechanics and Engineering. His research mainly focuses on intelligent construction method for underground space, digital twin technology for rock engineering, automated perception of rock geological information, multi-modal AI model for tunnel engineering, and discontinuous deformation analysis.